

Passive Inference Attacks on Split Learning via Adversarial Regularization

Xiaochen Zhu
National University of Singapore
xczhu@nus.edu.sg

Xinjian Luo
National University of Singapore
xinjluo@comp.nus.edu.sg

Yuncheng Wu
National University of Singapore
wuyc@comp.nus.edu.sg

Yangfan Jiang
National University of Singapore
yangfan.jiang@comp.nus.edu.sg

Xiaokui Xiao
National University of Singapore
xkxiao@nus.edu.sg

Beng Chin Ooi
National University of Singapore
ooibc@comp.nus.edu.sg

ABSTRACT

Split Learning (SL) has emerged as a practical and efficient alternative to traditional federated learning. While previous attempts to attack SL have often relied on overly strong assumptions or targeted easily exploitable models, we seek to develop more practical attacks. We introduce SDAR, a novel attack framework against SL with an honest-but-curious server. SDAR leverages auxiliary data and adversarial regularization to learn a decodable simulator of the client’s private model, which can effectively infer the client’s private features under the vanilla SL, and both features and labels under the U-shaped SL. We perform extensive experiments in both configurations to validate the effectiveness of our proposed attacks. Notably, in challenging but practical scenarios where existing passive attacks struggle to reconstruct the client’s private data effectively, SDAR consistently achieves attack performance comparable to active attacks. On CIFAR-10, at the deep split level of 7, SDAR achieves private feature reconstruction with less than 0.025 mean squared error in both the vanilla and the U-shaped SL, and attains a label inference accuracy of over 98% in the U-shaped setting, while existing attacks fail to produce non-trivial results.

1 INTRODUCTION

To bridge the isolated data repositories across different data owners, federated learning (FL) [24, 29, 32, 53, 54, 57] has been proposed as a solution to privacy-preserving collaborative learning. However, participants engaged in FL often suffer from low communication efficiency and heavy computational overhead imposed by the iterative process of local model training and the frequent exchange of model parameters, especially when the local models to be trained are deep neural networks (NNs). Naturally, as a simple adaption with enhanced communication and computation efficiency of FL, split learning (SL) [18, 37, 40, 43, 47, 48, 59] has drawn increasing attention in various applications, such as healthcare [19, 48] and open source packages [20, 38]. The general idea of SL is to *split* an NN model into smaller partial models, with simpler models being allocated to clients, and more intricate ones hosted on a computationally capable server. During training, clients send the intermediate representations produced by their partial models to the server, which subsequently performs a forward pass utilizing its own partial model and back-propagates the gradients back to the

clients to perform model updates. In this way, SL enables privacy-preserving collaborative learning by sharing only the intermediate representations without revealing the original private data from the clients. Compared to FL, SL adopts a more computationally efficient approach, yielding improved communication efficiency and scalability without compromising model utility [14, 43, 59]. Nonetheless, privacy concerns still exist within the SL framework. Given that clients share model intermediate representations with the server, one may naturally wonder *if it is possible for the server to infer private data of clients from the shared intermediate representations*.

Related work. To address this question, several inference attacks [9, 13, 22, 39, 41, 60] have been devised to investigate the privacy risks of SL. However, *these attacks typically consider impractical threat models and target non-standard settings favorable for the adversary*. For example, Pasquini et al. [39] assume a malicious server that *actively* tampers the back-propagated gradients, which deviates from the original training protocol of SL and can be easily detected as an agreement violation [8, 12]. In addition, Erdoğan et al. [9] and Gao and Zhang [13] propose passive inference attacks, in which the server honestly follows the SL training protocol but attempts to infer clients’ private data by analyzing the shared intermediate outputs. Although these two attacks are more stealthy, they also target non-standard and easily exploitable models, as did in [39]. Specifically, the targeted models on the clients’ side are typically non-standard models that are overly wide for their input dimensions, which results in higher dimensional intermediate representations encoding more information about the private input, thus making the attacks more effective. Additionally, existing attacks are often evaluated on split configurations where the clients’ models are shallow, which are commonly believed to be more vulnerable to attacks [13, 39, 49]. Correspondingly, these attacks can be defended by considering models with adequate width and allocating more layers to the clients’ partial models. Furthermore, the visual features of reconstructed images produced by existing passive attacks are hardly comparable to that of the active attack proposed by Pasquini et al. [39]. Therefore, it is still underexplored whether passive inference attacks can achieve reasonable effectiveness in practical SL scenarios involving less exploitable model structures. Please refer to Appendix A for detailed discussions on related work.

In this paper, we address this gap by developing passive feature and label inference attacks on practical SL settings where existing attacks [9, 13, 39] fail to work, i.e., we target standard models with adequate width at deeper split levels. By considering passive attacks, we can ensure the stealthiness of our attacks, making them hardly



susceptible to detection by active defense mechanisms [8, 12]. By considering the practical SL settings, we can reveal the privacy vulnerabilities that may exist in real-world applications but have not been explored. Nonetheless, before devising the proposed attacks, several challenges must be addressed.

Challenges. First, the main challenge in server-side attacks on SL is the absence of access (including the black-box access) to the client’s partial model, which means that the server cannot feed specific input to the client’s model and observe the corresponding output, rendering the traditional approach of model inversion [10, 11, 62] inapplicable. Second, in a passive setting where the server cannot manipulate the client’s model, the only information available to the server is the shared intermediate representations. As the complexity of the client’s partial model increases, e.g., with deeper split levels, the information encoded in these intermediate representations diminishes, making it more challenging to decode the private data solely from the received representations. Third, during SL training, the client’s model undergoes continuous updates in each iteration. This dynamic nature results in entirely different representations over iterations, further complicating inference attacks for the server, compared to attacks on finalized models [22, 60].

Aside from the typical SL setting, we also consider a more intricate SL configuration, known as U-shaped SL, where the last few layers of the model are also kept privately by the clients, and the server’s responsibility is limited to training the intermediate layers of a neural network. This introduces two new challenges. First, the absence of access to training examples’ labels poses the need for the server to simultaneously recover private features and labels to achieve a reasonable attack. Second, established practices and theoretical insights of transfer learning indicate that the last few layers of a network are crucial to learn domain-specific representations [61], and the lack of these layers makes it harder for the server to recover private training samples than in vanilla SL.

Contributions. To address these challenges, we propose a novel class of passive attacks on SL, namely, Simulator Decoding with Adversarial Regularization (SDAR). The basic idea behind SDAR involves the server initially training a simulator that emulates the client’s private model and subsequently training a decoder tailored to the trained simulator, with the help of auxiliary data disjoint from the private target data [13, 39]. The rationale of SDAR is that a well-trained decoder should be capable of decoding the intermediate representations generated by the client’s private model. However, due to the intrinsic differences in distribution between the client’s private data and the server’s auxiliary data, the simulator trained by the server tends to overfit the auxiliary data. Consequently, the simulator cannot faithfully replicate the behaviors of the client’s model, resulting in the decoder being proficient at decoding the auxiliary data but incapable of decoding the client’s private data.

To solve this issue, we draw inspiration from generative adversarial networks (GANs) [15, 16] and innovatively propose to regularize the simulator and decoder through an adversarial loss, encouraging them to learn more generalized representations that are transferable to the client’s private data. For vanilla SL where the server has access to the labels of training records, SDAR utilizes the label information in the style of conditional GAN [33]. In the more challenging U-shaped SL setting, where the client privately

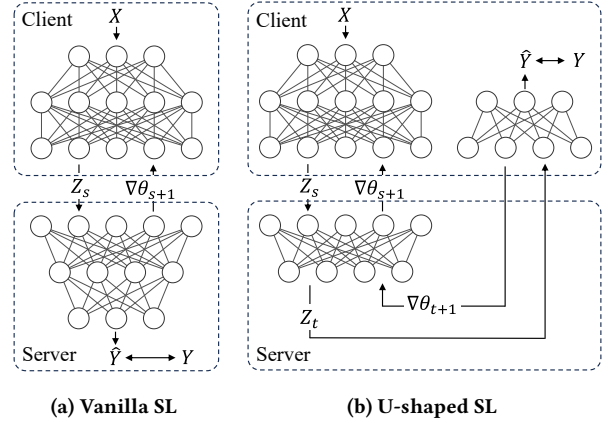


Figure 1: Vanilla and U-shaped configurations of SL.

retains the last few layers of the model along with the record labels, SDAR trains an additional simulator to mimic the behavior of these last few layers. To mitigate overfitting of this supplementary simulator, we introduce label random flipping, which encourages this simulator to learn the general representations rather than mere memorization of the server’s data. Furthermore, we utilize the inference outcomes of this simulator on private samples to achieve label inference attacks in the context of the U-shaped setting.

We conduct extensive experiments on various real-world datasets in both SL configurations to demonstrate the effectiveness of the proposed attacks. The results show that under challenging yet practical settings where existing attacks fail to effectively reconstruct clients’ private data, SDAR achieves consistent and distinctive attack performance. In addition, we evaluate potential countermeasures and show the robustness of our attacks against such defenses.

2 PRELIMINARIES

Split learning. We consider training an NN model H on dataset $D = \{(x_t, y_t) : t = 1, \dots, N\}$. H consists of n layers $H = L_n \circ L_{n-1} \dots \circ L_1$. The key idea of SL [18, 40, 48] is to *split* the execution of H by a *split layer* (namely, L_s) and assign the first half $f = L_s \circ \dots \circ L_1$ to the client and the second half $g = L_n \circ \dots \circ L_{s+1}$ to the server. Then, $H = g \circ f$. In the vanilla SL setting, the server also holds the labels of training examples. For a batch of examples X , define the representations returned by layer L_i as Z_i . Then, on the forward pass, the client sends intermediate representations $Z_s = f(X)$ (also known as smashed data) to the server such that the latter can complete the forward pass via $Z_n = g(Z_s)$. Since the server has access to the record labels Y , it can evaluate the loss $\ell(Z_n, Y)$ where $\ell(\cdot, Y)$ is the loss function given ground truth labels Y . In backpropagation, for parameters θ_i of L_i , chain rule gives

$$\nabla \theta_i = \frac{\partial \ell(Z_n, Y)}{\partial Z_n} \cdot \frac{\partial L_n(Z_{n-1})}{\partial \theta_n} \dots \frac{\partial L_i(Z_{i-1})}{\partial \theta_i} = \nabla \theta_{i+1} \frac{\partial L_i(Z_{i-1})}{\partial \theta_i}. \quad (1)$$

By (1), one only needs the gradients of the next layer and the representations returned by the previous layer to differentiate layer L_i . Thus, the server can update parameters θ_g of its model g after receiving Z_s from the client, while the client can update f after receiving $\nabla \theta_{s+1}$ from the server (see Fig. 1a for an example).

U-shaped SL. If the client’s record labels are considered private and not shared with the server, SL can be configured as a U-shaped structure [18], as illustrated in Fig. 1b. Under U-shaped SL, the NN

model is partitioned into three parts, i.e., $H = h \circ g \circ f$, where $f = L_s \circ \dots \circ L_1$, $g = L_t \circ \dots \circ L_{s+1}$, and $h = L_n \circ \dots \circ L_{t+1}$. The client owns f and h while the server only hosts g . During the training on samples X , the client sends Z_s to the server, which computes Z_t and sends it back to the client. The client then computes the final prediction $Z_n = h(Z_t)$. In the backpropagation phase, the client first updates its model h and sends $\nabla\theta_{t+1}$ to the server. Then, the server updates g and sends $\nabla\theta_{s+1}$ to the client for updating the partial model f on the client side.

SL with multiple clients. Due to its simplicity, the SL framework can be easily scaled to support multiple clients on either horizontally-partitioned data [48] or vertically-partitioned data [5]. Note that in the multi-client SL scenarios, each client still needs to communicate with the server via the above-described protocol, i.e., sharing intermediate representations with the server.

3 PROBLEM STATEMENT

System model. For ease of presentation, we introduce the proposed attacks in the SL setting where a client and a server collaboratively train a deep model H in either the vanilla or the U-shaped configuration. Our attacks can be seamlessly extended to the multi-client SL scenario for inferring the private data from different clients without further modifications, given that the shared information between clients and the server in the multi-client scenario is the same as that in the single-client scenario. Note that image datasets are typically used to train deep models under various SL settings [18].

Threat model. We investigate the privacy risks of SL under the honest-but-curious threat model [31], i.e., the server honestly adheres to the SL protocol and does not tamper with the training process but tries to passively infer the client’s private information from the received messages. In addition, we assume that the server has background knowledge of an auxiliary public dataset $D' = \{(x'_t, y'_t) : t = 1, \dots, m\}$ such that $D \cap D' = \emptyset$, where D denotes the client’s private dataset and shares a similar distribution with D' . This is a common and reasonable assumption in related studies [13, 39] because the task types and data domain should be negotiated between the client and the server before initiating an SL training. Consequently, the server can collect a public dataset from the same data domain for attack implementation [13, 39]. Note that we assume no access to any example in the client’s private dataset D for the server, which is more stringent than [13] where D' can be a subset of D . In addition, the server and the client should agree on the model architecture of H and the split configuration beforehand for information exchange and model convergence [9]. Therefore, we start by assuming that the server knows the architecture of f . We later relax this in App. D.3, assuming that the server does not have any knowledge of the architecture of f , but only the input and output dimensions of the model. During model training, the server has neither black-box nor white-box access to the client’s models, and can only receive intermediate representations from the client based on the SL protocol.

In *vanilla SL*, the client hosts model f while the server hosts model g and has access to the record labels. For a batch of training records (X, Y) , the server aims to reconstruct the private features X given the received intermediate representations Z_s , i.e., $\hat{X} = \mathcal{A}(Y, Z_s, \theta_g, D')$, where \hat{X} is the inferred features, θ_g represents

the parameters of g , and \mathcal{A} denotes the attack algorithm. In *U-shaped SL*, the client hosts partial models f and h while the server hosts model g . For a batch of training records (X, Y) , the server aims to reconstruct both the private features X and the labels Y given the received Z_s and the gradient vector $\nabla\theta_{t+1}$, i.e., $\hat{X}, \hat{Y} = \mathcal{A}(Z_s, \theta_g, \nabla\theta_{t+1}, D')$.

4 PASSIVE ATTACKS AGAINST SL

In this section, we introduce SDAR, a novel framework for an honest-but-curious server to infer the client’s private data in SL. The core idea of SDAR is using adversarial regularization to train a simulator model that learns similar representations as the client model in a way that the simulator’s outputs and the client model’s outputs are indistinguishable from each other by an adversarial discriminator. After that, a corresponding decoder is trained on D' for decoding the intermediate representations output by the simulator. By regularizing this decoder via an additional adversarial discriminator, this decoder can be generalized to effectively decode the client’s intermediate representations despite $D \cap D' = \emptyset$. SDAR is capable of inferring private features in the vanilla SL and both the private features and labels in the U-shaped SL, under challenging scenarios where the client’s model is deep and narrow.

4.1 Feature inference attacks in vanilla SL

We start with a simple attack prototype, denoted as naïve simulator decoding attack (naïve SDA). As the server has access to an auxiliary dataset D' and the knowledge of the architecture of the client’s f , it can first initialize a simulator \tilde{f} on its own with the same architecture as f (but with random initialization) and then train the model $g \circ \tilde{f}$ on D' . Specifically, for each batch of training examples (X, Y) , after the parameters of f, g are updated via the training loss $\ell(g(f(X)), Y)$, the server samples another batch of examples (X', Y') from D' and trains \tilde{f} to minimize loss $\ell(g(\tilde{f}(X')), Y')$ with the model g frozen. The reason to fix g in this step is mainly twofold. First, as an honest-but-curious party, the server should ensure that the parameters of g are only updated based on D as specified in the SL protocol. Second, fixing g while training \tilde{f} forces \tilde{f} to learn representations that are compatible with g . As g is trained collaboratively with the client’s model f on D , it is expected to memorize information of D [42] which may be implicitly leaked to \tilde{f} while training $g \circ \tilde{f}$. In this way, the encoder \tilde{f} trained by the server is expected to mimic the behaviors of f . In the meantime, the server trains a decoder \tilde{f}^{-1} with the transposed architecture of \tilde{f} to decode $Z'_s = \tilde{f}(X')$, i.e., the decoder parameters $\theta_{\tilde{f}^{-1}}$ are updated via the loss $\ell_{\text{MSE}}(X', \tilde{f}^{-1}(Z'_s))$. One may expect the decoder \tilde{f}^{-1} can not only decode the output of the simulator \tilde{f} but also effectively decode the output Z_s of f , i.e., $\tilde{f}^{-1}(Z_s) \approx X$ for private features X .

Unfortunately, the naïve SDA fails to achieve this objective as illustrated in Fig. 2a. The main reason behind the failure of naïve SDA is that although the training loss of $g \circ \tilde{f}$ on X' converges to a similar minimum as that of $g \circ f$ on X (see Fig. 2b), \tilde{f} fails to learn the same representations as f . This generalization gap is rooted in the distributional discrepancy between the disjoint datasets D and D' , and the fact that \tilde{f} is trained solely on D' makes it prone to overfitting to D' . As a result, even if the decoder \tilde{f}^{-1} can precisely

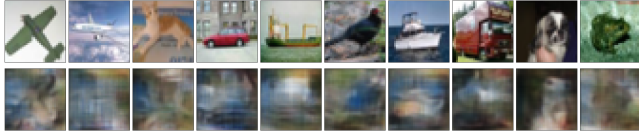
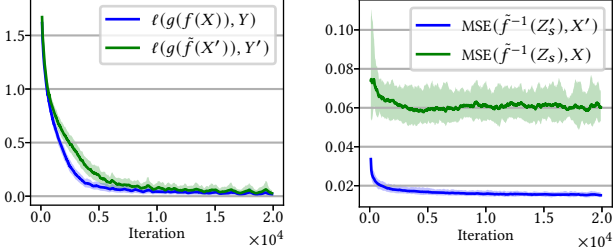
(a) Private X (upper) vs \hat{X} (lower) reconstructed by the naïve SDA(b) Training loss of $g \circ f$ vs $g \circ \tilde{f}$ (c) Decoding MSE on Z'_s vs Z_s

Figure 2: Failure of naïve SDA on CIFAR-10 with ResNet-20 at split level 7. Solid lines are mean values over 5 runs, and values between min/max boundaries are shaded. If not specified otherwise, all figures follow the same convention.

decode the simulator \tilde{f} with very low reconstruction error, its reconstruction error on Z_s , the output of the client’s private model f on unseen features X , does not converge (see Fig. 2c).

In response, we propose to enhance naïve SDA with adversarial regularization, to encourage the simulator and the decoder to learn more general representations transferable to the private data X .

Adversarial regularization for \tilde{f} . To regularize the simulator \tilde{f} such that it behaves more similarly to the client’s private model f , we introduce a server-side discriminator d_1 that is trained to distinguish $Z'_s = \tilde{f}(X')$ (the fake data) against $Z_s = f(X)$ (the real data). In each iteration, d_1 is updated to minimize the loss

$$\mathcal{L}_{d_1} = \ell_{\text{BCE}}(d_1(Z'_s), 0) + \ell_{\text{BCE}}(d_1(Z_s), 1) \quad (2)$$

to correctly classify Z'_s against Z_s , where ℓ_{BCE} is the binary cross-entropy loss. In the meantime, the simulator is updated in an adversarial way that maximizes the likelihood of being misclassified by the discriminator, i.e., to minimize the loss $\ell_{\text{BCE}}(d_1(\tilde{f}(X')), 1)$. We introduce this adversarial loss as a regularization term with penalty parameter λ_1 , i.e., the simulator \tilde{f} is updated to minimize the loss

$$\mathcal{L}_{\tilde{f}} = \ell(g(\tilde{f}(X')), Y') + \lambda_1 \cdot \ell_{\text{BCE}}(d_1(\tilde{f}(X')), 1). \quad (3)$$

Thus, with the training loss on D' as the main objective and the adversarial loss as the regularization term, the simulator is expected to output representations indistinguishable from the output of f , thus better simulating f ’s behaviors on the private data X .

Adversarial regularization for \tilde{f}^{-1} . As shown in Fig. 2c and 2a, the decoder \tilde{f}^{-1} can accurately decode the output of \tilde{f} since \tilde{f}^{-1} is trained in a supervised manner on Z'_s . However, this reconstruction capability can not be generalized to decode Z_s . Specifically, we observe from Fig 2a that the reconstructed samples \hat{X} exhibit obfuscated visual features and can be easily distinguished from real images by a well-trained discriminator. Motivated by this observation, we introduce another discriminator d_2 to distinguish $\tilde{f}^{-1}(Z_s)$ (the fake data) against X' (the real data) owned by the

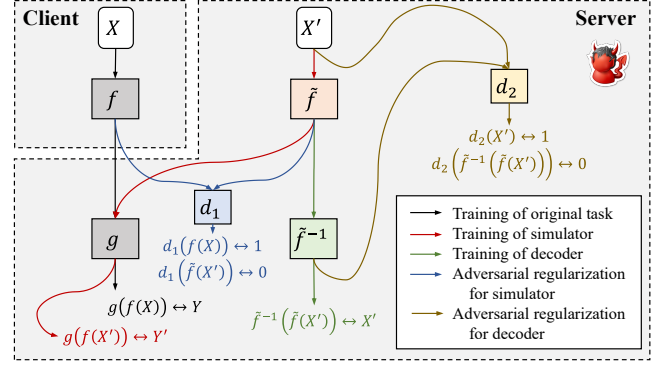


Figure 3: Overview of SDAR in the vanilla setting.

server. Similar to Eq. (2), d_2 is trained by minimizing

$$\mathcal{L}_{d_2} = \ell_{\text{BCE}}(d_2(\tilde{f}^{-1}(Z_s)), 0) + \ell_{\text{BCE}}(d_2(X'), 1). \quad (4)$$

Meanwhile, the decoder \tilde{f}^{-1} needs to be trained in an adversarial manner to maximize the likelihood of being misclassified by the discriminator. Similar to Eq. (3), we introduce a regularization term with penalty parameter λ_2 , and the decoder is trained to minimize

$$\mathcal{L}_{\tilde{f}^{-1}} = \ell_{\text{MSE}}(X', \tilde{f}^{-1}(Z'_s)) + \lambda_2 \cdot \ell_{\text{BCE}}(d_2(\tilde{f}^{-1}(Z_s)), 1). \quad (5)$$

In this way, the decoder is trained to reconstruct private images from Z_s with plausible visual features as real images.

Use of labels. In the vanilla SL, the server holds labels of all private training images, indicating that the server has access to the labels of both the private data X and the auxiliary data X' . This enables the server to adopt the decoder \tilde{f}^{-1} and the discriminators d_1, d_2 in a conditional manner similar to the conditional GANs [33]. Take the decoder \tilde{f}^{-1} as an example. Instead of only taking the intermediate representations Z_s, Z'_s as the input, a conditional \tilde{f}^{-1} can additionally take the corresponding labels Y, Y' as the input. These labels can be first transformed into a high-dimensional embedding and then concatenated with the intermediate representations. A similar modification can be applied to the discriminators. This adaptation enables the decoder to more effectively decode the intermediate representations, while also enhancing the discriminators’ capability to distinguish between real and synthetic examples.

With the integration of the aforementioned enhancements, we denote the refined simulator decoding attack as Simulator Decoding with Adversarial Regularization (SDAR). We describe the complete attack algorithm (Algorithm 1) in Appendix B and Figure 3.

4.2 Feature & label inference attacks in U-shaped SL

In the U-shaped SL, the model H is split into three parts $H = h \circ g \circ f$ such that only the intermediate partial model g is kept by the server, and the other two are trained by the client. An intuitive approach to adapt SDAR to the U-shaped SL is that the server trains an additional simulator \tilde{h} to mimic the behaviors of h , which can be updated by minimizing the training loss of $\tilde{h} \circ g \circ \tilde{f}$ on D' when freezing g . If the simulator \tilde{h} is well-trained on D' such that it is able to generalize well to classify unseen private examples in D , the server can effectively reconstruct private labels $\hat{Y} = \tilde{h}(g(Z_s))$ in addition to private features. However, the last few layers (i.e., h)

of the model has a strong expressive capacity of the private information suggested by the practice and theory of transfer learning [61]. Consequently, \tilde{h} can easily overfit to D' such that the training loss on D' converges to a local minimum yet \tilde{h} and \tilde{f} fail to learn the similar behaviors of h and f . In this case, the decoder \tilde{f}^{-1} will not be able to reconstruct the private input X from Z_s effectively when trained along with the overfitted \tilde{f} . Thus, it is crucial to ensure that the simulator \tilde{h} learns the general and transferable data representations, instead of overfitting to D' .

To this end, we introduce **random label flipping** in the training of $\tilde{h} \circ g \circ \tilde{f}$. Specifically, for each batch of examples (X', Y') sampled from D' , we first randomly modify a small fraction of Y' to new random labels for generating a new label set \tilde{Y}' . After that, we train $\tilde{h} \circ g \circ \tilde{f}$ based on the new training batch (X', \tilde{Y}') . The rationale is that the randomly flipped labels can help regularize the training of \tilde{h} , enabling \tilde{h} to produce more general data representations that are compatible with the output of g and meanwhile transferable to the private data D . Other components of SDAR except for the use of labels in Sec. 4.1 are directly applicable to the U-shaped SL setting, including the adversarial regularization on \tilde{f} and \tilde{f}^{-1} . We describe the complete attack algorithm (Algorithm 2) in Appendix B.

4.3 Technical novelty

First, SDAR identifies an underexplored vulnerability of SL, i.e., the risks of information leakage from the parameters of the server's model g . Since g is trained together with f on the private examples (X, Y) , it unintentionally memorizes information about the private data [42], and a carefully designed simulator trained with g and (X', Y') can accurately simulate the behaviors of f . On the contrary, most existing attacks [9, 39] focus on only exploiting the privacy risks of the client's intermediate representations Z_s , which is often insufficient to reconstruct private data under practical settings.

Second, SDAR utilizes a novel adversarial regularization method to considerably improve the generalization performance of the simulator and decoder on the client's private data, which can achieve consistent and robust attack performance on less vulnerable models where existing attacks [9, 13, 39] cannot work. To the best of our knowledge, this is also the first time that adversarial regularization is utilized in the design of inference attacks on SL.

Note that one parallel study, PCAT [13], adopts a similar attack framework as our naïve SDA discussed in Sec. 4.1, with some minor improvements. However, as demonstrated in Fig. 2 and our comparative experiments in Sec. 5, PCAT fails to reconstruct reasonable images in challenging but practical settings.

5 EXPERIMENTS

5.1 Experimental settings

Datasets. We experiment with 4 popular benchmarking datasets: Fashion-MNIST [55], CIFAR-10 [27], CIFAR-100 [27], and Tiny ImageNet [1]. Due to limited space, we report results on CIFAR-10 and CIFAR-100 in the main text, and defer full results to Appendix G. We resize the former three datasets to $32 \times 32 \times 3$ images to match the input configuration of ResNet-20 [21], and keep Tiny ImageNet's original size of $64 \times 64 \times 3$ to demonstrate the attack's scalability to larger images. All images are normalized to $[0, 1]$ beforehand to match the input configuration of ResNet-20 [21]. We partition

Table 1: Model statistics on different split levels in vanilla SL.

Level	#layers of f	#param. of f	#layers of g	#param. of g
3	7	14,704	13	259,338
4	9	29,424	11	244,618
5	11	48,112	9	225,930
6	13	66,800	7	207,242
7	15	124,912	5	149,130

each dataset into two disjoint subsets D, D' where D belongs to the client, and D' belongs to the server. We start with $|D| = |D'|$ where the server acquires auxiliary data of the same size as the client's private dataset. Then, we experiment with $|D'| \ll |D|$ to discuss the effectiveness of our attacks with much less data.

Models. We use ResNet-20 [21] as the base model architecture for H , a standard model specifically designed to classify the CIFAR datasets. We chose residual networks because they are widely adopted in real-world applications, and are recognized to be hard to invert [3]. H consists of 20 layers (19 convolutional layers and one additional fully-connected output layer), with 9 residual blocks. We experiment with different split levels denoted by $s \in \{3, 4, 5, 6, 7\}$ on the ResNet-20 model, characterized by the number of residual blocks in the client's model f . The deepest client's model has 7 residual blocks as adding any more blocks will render the client to host more parameters than the server, invalidating SL's purpose of enabling a powerful server to relieve the client from heavy computation. In the vanilla SL, all the remaining layers are assigned to the server as shown in Table 1. In the U-shaped SL, the last few layers, including the average pooling and the fully connected output layer, are also assigned to the client, while the server only hosts the layers in between. By considering the standard ResNet-20 model with 16/32/64 filters and deep split levels up to 7, we target more challenging and practical settings where the client's private model is less exploitable to existing attacks. Our experiments demonstrate that the wider and shallower models considered by existing attacks [9, 13, 39] are more vulnerable to our attacks.

For the simulator \tilde{f} (and \tilde{h} if in U-shaped SL) of SDAR, we start with the case where the server uses the same model architecture as that of the client's f (and h if in U-shaped SL). We later show that our attacks are still effective even without such information where the simulator has a different architecture. The server uses the decoder \tilde{f}^{-1} with a structure transposed to \tilde{f} ending with a sigmoid function to produce tensors within $[0, 1]$. The discriminators d_1 that distinguishes Z'_s from Z_s , and d_2 that distinguishes \hat{X} from X' , are deep convolutional networks. Architecture details of the attack models are described in Appendix F.3.

Baselines. We compare SDAR with existing attacks, including UnSplit [9], PCAT [13] and FSHA [39]. UnSplit [9] is a passive attack which reconstructs private features by minimizing $\ell_{\text{MSE}}(\tilde{f}(\hat{X}), Z_s)$ via alternating optimization on \tilde{f} and \hat{X} . PCAT [13] is also a passive attack that adopts a similar attack framework as our naïve SDA discussed in Sec. 4.1. FSHA [39], on the other hand, is an active attack framework, where the server actively hijacks the gradients transmitted to the client such that the client's model f is induced to behave similarly to the server's own encoder. To ensure the fairness of comparison, we use the same model architectures and auxiliary

Table 2: Mean values with standard deviations of the reconstruction MSE over 5 trials on CIFAR-10 in the vanilla SL.

Level	SDAR	PCAT [13]	UnSplit [9]
3	0.0059 (0.0005)	0.0202 (0.0026)	0.0688 (0.0027)
4	0.0104 (0.0009)	0.0237 (0.0021)	0.0662 (0.0004)
5	0.0120 (0.0003)	0.0337 (0.0048)	0.0670 (0.0000)
6	0.0134 (0.0007)	0.0382 (0.0062)	0.0674 (0.0005)
7	0.0216 (0.0014)	0.0568 (0.0062)	0.0660 (0.0000)

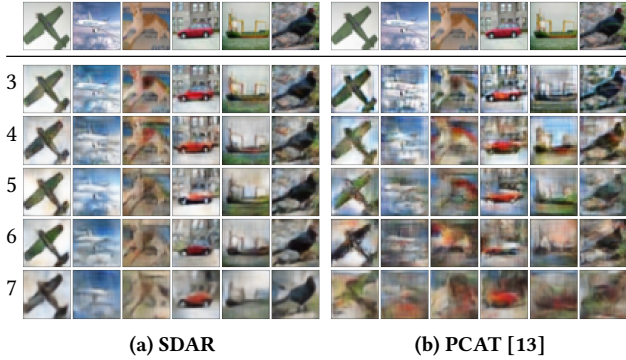


Figure 4: Examples of feature inference attack results on CIFAR-10 in vanilla SL. The first row shows the original private images while the following rows show the reconstructed images by SDAR and PCAT at various split levels 3–7. Reconstructions of the best quality among 5 trials are shown.

datasets in different attacks. Implementation details of the baselines are described in Appendix F.3.1.

5.2 Experiments on vanilla SL attacks

Attack effectiveness. We report the results of SDAR and other passive feature inference attacks on CIFAR-10 at split levels 3–7 in Table 2 and give concrete examples of private data reconstruction in Fig. 4. Table 2 demonstrates that the proposed attack, SDAR, surpasses existing passive attacks [9, 13] in terms of reconstruction errors at all split levels by a significant margin. We note that SDAR achieves nearly perfect reconstruction at shallower split cuts, and is still able to achieve exceptional reconstruction quality even at deep split levels up to 7 (see Fig. 4). PCAT [13] is able to recover private features at shallower split levels (≤ 4) but of much lower quality than SDAR. In particular, the reconstruction quality of PCAT in the most trivial case (split level 3) is even worse than the attack results of SDAR at the deepest split level 7. Moreover, the effectiveness of PCAT degenerates dramatically at deeper split levels, resulting in even larger performance gaps compared to SDAR. This is demonstrated in Fig. 4 where PCAT struggles to produce reasonable reconstruction at split levels 6–7. We note that the images reconstructed by UnSplit [9] are indistinguishable at all split levels and are thus omitted in this paper. The performance of UnSplit is expected as $\hat{f}(\hat{X}) \approx f(X)$ does not necessarily lead to $\hat{X} \approx X$.

Comparison to active attacks. We also compare SDAR with the SOTA active feature inference attack, FSHA [39], and report the attack MSE curve over training iterations at split level 7 on CIFAR-10 in Fig 5a. Note that as an active attack where the server actively hijacks the client’s gradients to manipulate the training of f ,

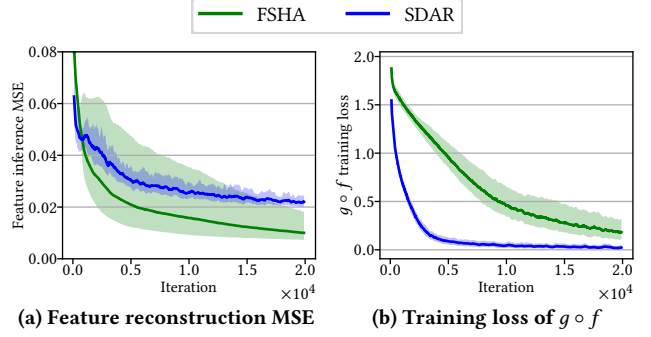


Figure 5: Attack MSE and training losses on the original task of SDAR vs FSHA on CIFAR-10 at split level 7 in vanilla SL.

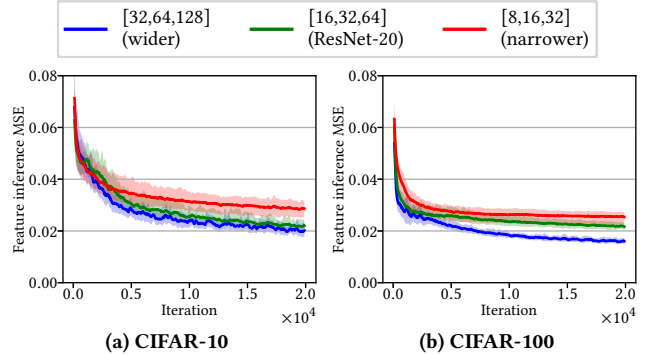


Figure 6: Effects of target model width on SDAR performed on CIFAR-10 and CIFAR-100 at split level 7 in vanilla SL.

FSHA is expected to exhibit substantially better attack performance than passive attacks. Yet, we observe that our attack, despite being passive, still can achieve comparable attack performance as FSHA. This indicates the strong capability of our proposed attack, which is unprecedented in existing passive attacks. A particular advantage of SDAR is the preservation of the original training task as the server does not tamper with the SL training protocol. This is demonstrated in Fig. 5b where SDAR’s training loss of $g \circ f$ on X converges much faster than FSHA. Consequently, SDAR poses a greater risk to real-world applications compared to FSHA, as the original training task is preserved and the server can perform the attack of robust quality without being detected by the client [8, 12].

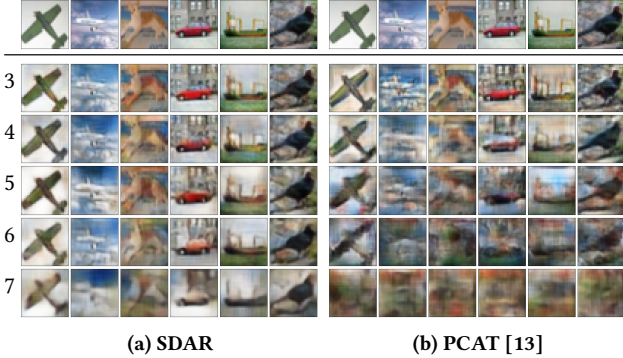
Effects of target model width. We have shown that deeper target model f is less vulnerable to inference attacks, and we discuss the effects of model width (number of filters) on the attack performance of SDAR in Fig. 6. Since ResNet-20 uses convolutional layers of 16/32/64 filters, we experiment with wider and narrower models by doubling and halving filters in each layer. It can be seen that attack performance improves with model width. This is because wider models output Z_s of significantly larger dimensions, encoding more information about the private training data. It is worth noting that existing attacks [9, 13, 39] are often evaluated on *overly wide models at shallower split levels*, which, as discussed, are much easier to attack. For example, PCAT [13] is evaluated on a CNN model with up to 512 filters for $32 \times 32 \times 3$ images in CIFAR-10, with the deepest split level of merely four convolutional

Table 3: Ablation studies on CIFAR-10 at level 7 in vanilla SL.

	d_1 (for \tilde{f})	d_2 (for \tilde{f}^{-1})	conditional	attack MSE
1	✓	✓	✓	0.0216 (0.0014)
2	✗	✓	✓	0.0575 (0.0036)
3	✓	✗	✓	0.0234 (0.0015)
4	✗	✗	✓	0.0607 (0.0093)
5	✓	✓	✗	0.0222 (0.0012)

Table 4: Mean values with standard deviations of feature reconstruction MSE and label inference accuracy over 5 trials on CIFAR-10 at split levels 3–7 in U-shaped SL.

lv.	Feature MSE		Label ACC (%)	
	SDAR	PCAT [13]	SDAR	PCAT [13]
3	0.0051 (0.0007)	0.0223 (0.0040)	98.15 (1.18)	98.13 (1.16)
4	0.0085 (0.0013)	0.0387 (0.0262)	98.61 (0.26)	88.66 (18.88)
5	0.0120 (0.0017)	0.0665 (0.0262)	98.49 (0.25)	58.11 (34.33)
6	0.0138 (0.0013)	0.0791 (0.0122)	98.15 (0.51)	21.34 (25.29)
7	0.0247 (0.0009)	0.0947 (0.0184)	98.71 (0.77)	15.45 (09.99)

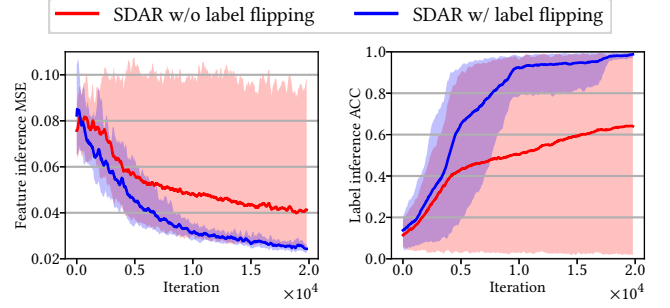
**Figure 7: Examples of feature inference attack results on CIFAR-10 in U-shaped SL. See Fig. 4 for detailed descriptions.**

layers allocated to the client. Our experiments with the standard ResNet-20 model demonstrate that SDAR is able to attack much less vulnerable models with significantly better performance.

Ablation studies. We conduct ablation studies in Table 3 to evaluate the effectiveness of each component in SDAR. We observe that all components are crucial, as removing any of them results in worse attack performance. In particular, attack performance degenerates the most when the server does not use adversarial regularization (case 4), showing its effectiveness to reduce overfitting and improve the generalization of the simulator/decoder. Between the two adversarial regularizers for \tilde{f} and \tilde{f}^{-1} , SDAR is more sensitive to the former (case 2 vs 3). Because the successful generalization of the decoder heavily relies on the quality of the simulator. At last, we notice a marginal performance gain by utilizing labels of the private examples in the style of CGANs [33] (case 1 vs 5), when the discriminators and decoders are fed with additional information.

5.3 Experiments on U-shaped SL attacks

Attack effectiveness. As SDAR can infer both features and labels of the client’s training examples, we report the feature reconstruction MSE and the label inference accuracy in Table 4, and

**Figure 8: Effects of random label flipping on SDAR on CIFAR-10 at split level 7 in U-shaped SL.**

present examples of private feature reconstructions in Fig. 7. Note that we no longer present results of UnSplit [9] due to its inability to produce distinguishable results even in the vanilla SL setting. Similar to feature inference attacks in vanilla SL, SDAR can reconstruct private features of high quality across various split levels, and there is no significant performance drop compared to vanilla SL. The reason is that although the server no longer has access to the last part of the model, i.e., h , it manages to train a simulator \tilde{h} that learns the same representations, as supported by the high label inference accuracy which consistently reaches around 98% on CIFAR-10 across all split levels. As the server trains $\tilde{h} \circ g \circ \tilde{f}$ solely on D' (while g is trained on D), its high test accuracy on unseen examples in D demonstrates that information about D is indeed leaked to the server via the trained parameters of g . In contrast, PCAT [13] achieves visibly worse feature reconstruction performance than in vanilla SL, since PCAT is unable to train an effective simulator to h , as supported by its poor label inference accuracy. It can be seen that with deeper split levels and fewer parameters in the server’s g , less information about D is leaked via g , and hence the label inference accuracy of PCAT dramatically degenerates to the level of random guessing when the split level increases to 7.

Effects of random label flipping. Many of the properties of SDAR in vanilla SL discussed in Sec. 5.2 directly apply to the U-shaped SL, and we focus on the effects of random label flipping on the training of \tilde{h} . Fig. 8 shows that after removing random label flipping, the label inference accuracy of SDAR drops significantly, and in the worst case, the label inference accuracy quickly vanishes to near-zero, even worse than random guessing. Thus, without label flipping, server’s model \tilde{h} will quickly overfit to its own dataset D' without simulating the behavior of h on D . As a result, the simulator \tilde{f} trained together with \tilde{h} will not learn the same representations as f and hence the decoder can no longer generalize to decode the client’s f , leading to poor feature inference performance as well. With random label flipping, the server’s model \tilde{h} is forced to learn the general representations over time instead of overfitting to D' .

5.4 Additional discussions

Furthermore, we evaluate SDAR in other metrics in App. D.1, demonstrate that SDAR is still effective with much less auxiliary data that does not share the same distribution of the client’s private data (in App. D.2) or without any knowledge of the client’s model architecture (in App. D.3), and explore multi-client settings in App. D.4.

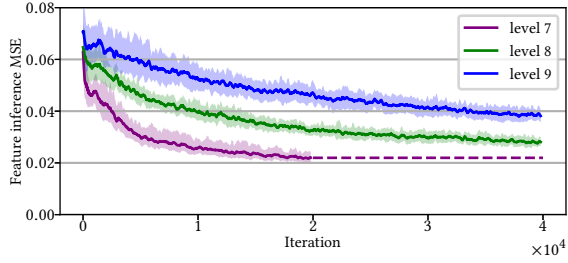


Figure 9: Attack MSE of SDAR on CIFAR-10 with ResNet-20 at deeper split levels of 7–9 in the vanilla SL configuration.

Table 5: Attack MSE of SDAR and training accuracies of SL on CIFAR-100 at split level 7 in vanilla SL with dropout.

Dropout rate	0.0	0.2	0.4	0.6	0.8
Attack MSE	0.0217 (0.0011)	0.0222 (0.0014)	0.0227 (0.0011)	0.0245 (0.0020)	0.0263 (0.0020)
Train ACC (%)	96.24 (0.65)	91.33 (0.29)	86.08 (0.38)	74.13 (0.82)	40.33 (0.73)

Table 6: Attack MSE of SDAR on CIFAR-10 at split level 7 in vanilla SL at different ℓ_1/ℓ_2 regularization factors.

Regularization factor	0.0	0.001	0.01	0.1
Attack MSE on SL with ℓ_1 regularization	0.0216 (0.0014)	0.0219 (0.0009)	0.0222 (0.0016)	0.0230 (0.0028)
Attack MSE on SL with ℓ_2 regularization	0.0216 (0.0014)	0.0223 (0.0017)	0.0228 (0.0020)	0.0223 (0.0012)

6 POTENTIAL COUNTERMEASURES

Change of model architectures. We have demonstrated the effectiveness of SDAR on ResNet-20 (in Table 2 and Table 4) and its narrower variants (in Fig. 6) at the deep split level of seven and show that narrower models at deeper split levels are relatively more robust to our attacks. A natural defense against SDAR is to assign more layers to the clients’ model. Therefore, we conduct experiments at split levels up to 9 to observe the SDAR performance. The results are presented Fig. 9. Note that at split level 9, the client hosts all convolutional layers, and the server has merely 650 parameters. This is an extreme case that is not practical in real-world deployments, as this invalidates SL’s purpose of relieving the client’s computational burden with a capable server. From Fig. 9, we see that even at level 9, SDAR’s attack MSE continues to decrease over time without saturation. Therefore, we conclude that SDAR is robust against different split levels, and changing the model architecture is not a viable defense against our attacks.

Regularization. Overfitting is a key concern in inference attacks on ML models [34, 42], as ML models may overfit to and unintentionally memorize private training data. Dropout [31, 44] and ℓ_1/ℓ_2 regularization [35] are straightforward yet effective techniques to prevent overfitting. Therefore, we consider these two regularizers as a potential defense and evaluate SDAR against them. As shown in Table 5, the increase in dropout rate slightly degrades the attack performance of SDAR, but the attack MSE remains at a low level, indicating the attack effectiveness against dropout. Table 5 also

Table 7: Attack MSE of SDAR on CIFAR-100 in vanilla SL at split level 7 with decorrelation defense with various α values.

α	0.0	0.2	0.4	0.6	0.8
Attack MSE	0.0217 (0.0011)	0.0315 (0.0014)	0.0383 (0.0009)	0.0444 (0.0012)	0.0475 (0.0012)
Train ACC (%)	96.41 (1.36)	96.09 (1.10)	94.53 (1.10)	93.28 (1.89)	70.16 (6.54)

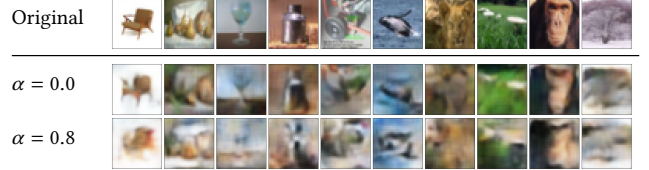


Figure 10: Examples of feature inference attack results on CIFAR-100 at split level 7 with decorrelation with $\alpha \in \{0, 0.8\}$.

shows that large dropout rates can lead to significant degradation in the training accuracy of SL. Similarly, we observe from Table 6 that variations of the ℓ_1/ℓ_2 regularization factors have limited influence on the attack performance. The reason that our attacks are robust against regularization defense is due to the fact that the same regularization is also applied in the training of the simulator, so the \hat{f} can simulate the regularized behavior of the client’s f . Therefore, dropout and ℓ_1/ℓ_2 regularization is not a viable defense.

Decorrelation. A recent method for enhancing the privacy of SL is to decorrelate the intermediate representations Z_s with the input private features X [49, 50]. This is done by replacing $g \circ f$ ’s loss function $\ell(g(f(X)), Y)$ with $(1 - \alpha)\ell(g(f(X)), Y) + \alpha \cdot \text{dCol}(f(X), X)$, where α is the decorrelation parameter and $\text{dCol}(\cdot, \cdot)$ is the distance correlation [45]. To evaluate the effectiveness of SDAR against this decorrelation defense, we first introduce a decorrelation term in Eq. (3) to decorrelate $\hat{f}(X')$ with X' in SDAR, such that the simulator can learn the decorrelation behaviors of client’s f . Then, we perform SDAR on SL with decorrelation with $\alpha \in \{0.2, 0.4, 0.6, 0.8\}$. As shown in Table 7 and Fig. 10, although decorrelation manages to degrade the attack quality when α increases, SDAR still produces visibly precise reconstructions even at $\alpha = 0.8$. Also, Table 7 shows that the decorrelation defense with larger α results in a notable loss in training accuracy of the original task, rendering this defense relatively impractical in real-world applications.

Others. Appendix E discusses additional potential defenses to our attacks and their inapplicability in SL in their current forms, including homomorphic encryption [46, 52], secure multi-party computation [4, 25, 53, 58], and differential privacy [2, 7, 56].

7 CONCLUSION

In this paper, we investigate the privacy risks of split learning under the notion of an honest-but-curious server. We identify that existing server-side passive attacks often target impractical and vulnerable settings to gain extra advantage for the adversary. We present new passive attacks on split learning, namely, SDAR, by utilizing GAN-inspired adversarial regularization to learn a decodable simulator of client’s private model that produces representations

indistinguishable from the client's. Empirically, we show that SDAR is effective in inferring private features of the client in vanilla SL, and both private features and labels in the U-shaped SL, under challenging settings where existing passive attacks fail to produce non-trivial results. At last, we propose and evaluate potential defenses against our attacks and highlight the need for improving SL to further protect the client's private data.

Split learning is a promising protocol to enable distributed training and inference of neural networks on devices with limited computational resources. There are many open challenges and potential directions regarding its security. For example, one may rigorously study the privacy guarantee of SL and theoretically measure the information leakage of the protocol. Also, it will be an interesting direction to design privacy-preserving mechanisms to mitigate our proposed attacks and improve the privacy of SL.

REFERENCES

- [1] [n. d.]. Tiny ImageNet. <http://cs231n.stanford.edu/tiny-imagenet-200.zip>. Accessed: 2023-12-28.
- [2] Martin Abadi, Andy Chu, Ian Goodfellow, H Brendan McMahan, Ilya Mironov, Kunal Talwar, and Li Zhang. 2016. Deep learning with differential privacy. In *CCS*. 308–318.
- [3] Jens Behrmann, Will Grathwohl, Ricky TQ Chen, David Duvenaud, and Jörn-Henrik Jacobsen. 2019. Invertible residual networks. In *ICML*. 573–582.
- [4] Keith Bonawitz, Vladimir Ivanov, Ben Kreuter, Antonio Marcedone, H Brendan McMahan, Sarvar Patel, Daniel Ramage, Aaron Segal, and Karn Seth. 2017. Practical secure aggregation for privacy-preserving machine learning. In *CCS*. 1175–1191.
- [5] Iker Ceballos, Vivek Sharma, Eduardo Mugica, Abhishek Singh, Alberto Roman, Praneeth Vepakomma, and Ramesh Raskar. 2020. SplitNN-driven Vertical Partitioning. *CoRR* abs/2008.04137 (2020).
- [6] TensorFlow Developers. 2023. *TensorFlow*. <https://doi.org/10.5281/zenodo.7604251>
- [7] Cynthia Dwork, Aaron Roth, et al. 2014. The algorithmic foundations of differential privacy. *Found. Trends Theor. Comput. Sci.* 9, 3–4 (2014), 211–407.
- [8] Ege Erdogan, Alptekin Küpçü, and A Ercument Cicek. 2022. Splitguard: Detecting and mitigating training-hijacking attacks in split learning. In *WPES*. 125–137.
- [9] Ege Erdoğan, Alptekin Küpçü, and A Ercument Çiçek. 2022. Unsplit: Data-oblivious model inversion, model stealing, and label inference attacks against split learning. In *WPES*. 115–124.
- [10] Matt Fredrikson, Somesh Jha, and Thomas Ristenpart. 2015. Model inversion attacks that exploit confidence information and basic countermeasures. In *CCS*. 1322–1333.
- [11] Matthew Fredrikson, Eric Lantz, Somesh Jha, Simon Lin, David Page, and Thomas Ristenpart. 2014. Privacy in pharmacogenetics: An End-to-End case study of personalized warfarin dosing. In *USENIX Security*. 17–32.
- [12] Jiayun Fu, Xiaojing Ma, Bin B. Zhu, Pingyi Hu, Ruixin Zhao, Yaru Jia, Peng Xu, Hai Jin, and Dongmei Zhang. 2023. Focusing on Pinocchio's Nose: A Gradients Scrutinizer to Thwart Split-Learning Hijacking Attacks Using Intrinsic Attributes. In *NDSS*.
- [13] Xinben Gao and Lan Zhang. 2023. PCAT: Functionality and Data Stealing from Split Learning by Pseudo-Client Attack. In *USENIX Security*. 5271–5288.
- [14] Yansong Gao, Minki Kim, Sharif Abuadba, Yeonjae Kim, Chandra Thapa, Kyuyeon Kim, Seyit A Camtepe, Hyoungshick Kim, and Surya Nepal. 2020. End-to-End Evaluation of Federated Learning and Split Learning for Internet of Things. In *SRDS*. 91–100.
- [15] Ian Goodfellow, Jean Pouget-Abadie, Mehdi Mirza, Bing Xu, David Warde-Farley, Sherjil Ozair, Aaron Courville, and Yoshua Bengio. 2014. Generative adversarial nets. In *NeurIPS*.
- [16] Ian Goodfellow, Jean Pouget-Abadie, Mehdi Mirza, Bing Xu, David Warde-Farley, Sherjil Ozair, Aaron Courville, and Yoshua Bengio. 2020. Generative adversarial networks. *Commun. ACM* 63, 11 (2020), 139–144.
- [17] Ishaan Gulrajani, Faruk Ahmed, Martin Arjovsky, Vincent Dumoulin, and Aaron C Courville. 2017. Improved training of wasserstein gans. In *NeurIPS*.
- [18] Otkrist Gupta and Ramesh Raskar. 2018. Distributed learning of deep neural network over multiple agents. *J. Netw. Comput. Appl.* 116 (2018), 1–8.
- [19] Yoo Jeong Ha, Gusang Lee, Minjae Yoo, Soyi Jung, Seehwan Yoo, and Joongheon Kim. 2022. Feasibility study of multi-site split learning for privacy-preserving medical systems under data imbalance constraints in COVID-19, X-ray, and cholesterol dataset. *Scientific Reports* 12, 1 (2022), 1–11.
- [20] Adam J Hall. 2020. *Implementing split neural networks on PySyft*. <https://blog.openmined.org/split-neural-networks-on-pysyft/>
- [21] Kaiming He, Xiangyu Zhang, Shaoqing Ren, and Jian Sun. 2016. Deep residual learning for image recognition. In *CVPR*. 770–778.
- [22] Zecheng He, Tianwei Zhang, and Ruby B Lee. 2019. Model inversion attacks against collaborative inference. In *ACSAC*. 148–162.
- [23] Geoffrey E Hinton and Ruslan R Salakhutdinov. 2006. Reducing the dimensionality of data with neural networks. *Science* 313, 5786 (2006), 504–507.
- [24] Peter Kairouz, H Brendan McMahan, Brendan Avent, Aurélien Bellet, Mehdi Bennis, Arjun Nitin Bhagoji, Kallista Bonawitz, Zachary Charles, Graham Cormode, Rachel Cummings, et al. 2021. Advances and open problems in federated learning. *Foundations and Trends® in Machine Learning* 14, 1–2 (2021), 1–210.
- [25] Marcel Keller. 2020. MP-SPDZ: A Versatile Framework for Multi-Party Computation. In *CCS*. 1575–1590.
- [26] Diederik P. Kingma and Jimmy Ba. 2015. Adam: A Method for Stochastic Optimization. In *ICLR*.
- [27] Alex Krizhevsky, Geoffrey Hinton, et al. 2009. Learning multiple layers of features from tiny images. (2009).
- [28] Oscar Li, Jiankai Sun, Xin Yang, Weihao Gao, Hongyi Zhang, Junyuan Xie, Virginia Smith, and Chong Wang. 2022. Label Leakage and Protection in Two-party Split Learning. In *ICLR*.
- [29] Bingyan Liu, Yao Guo, and Xiangqun Chen. 2021. PFA: Privacy-preserving federated adaptation for effective model personalization. In *WWW*. 923–934.
- [30] Junlin Liu and Xinchun Lyu. 2023. Clustering label inference attack against practical split learning. *CoRR* abs/2203.05222 (2023).
- [31] Xinjian Luo, Yuncheng Wu, Xiaokui Xiao, and Beng Chin Ooi. 2021. Feature inference attack on model predictions in vertical federated learning. In *ICDE*. 181–192.
- [32] Brendan McMahan, Eider Moore, Daniel Ramage, Seth Hampson, and Blaise Agüera y Arcas. 2017. Communication-efficient learning of deep networks from decentralized data. In *AISTATS*. 1273–1282.
- [33] Mehdi Mirza and Simon Osindero. 2014. Conditional Generative Adversarial Nets. *CoRR* abs/1411.1784 (2014).
- [34] Milad Nasr, Reza Shokri, and Amir Houmansadr. 2019. Comprehensive privacy analysis of deep learning: Passive and active white-box inference attacks against centralized and federated learning. In *S&P*. 739–753.
- [35] Andrew Y Ng. 2004. Feature selection, L1 vs. L2 regularization, and rotational invariance. In *ICML*.
- [36] Augustus Odena, Vincent Dumoulin, and Chris Olah. 2016. Deconvolution and checkerboard artifacts. *Distill* 1, 10 (2016), e3.
- [37] Seungeun Oh, Jihong Park, Praneeth Vepakomma, Sihun Baek, Ramesh Raskar, Mehdi Bennis, and Seong-Lyun Kim. 2022. LocFedMix-SL: Localize, Federate, and Mix for Improved Scalability, Convergence, and Latency in Split Learning. In *WWW*. 3347–3357.
- [38] OpenMinded. 2021. *PySyft*. <https://github.com/OpenMined/PySyft>
- [39] Dario Pasquini, Giuseppe Ateniese, and Massimo Bernaschi. 2021. Unleashing the tiger: Inference attacks on split learning. In *CCS*. 2113–2129.
- [40] Maarten G Poirot, Praneeth Vepakomma, Ken Chang, Jayashree Kalpathy-Cramer, Rajiv Gupta, and Ramesh Raskar. 2019. Split learning for collaborative deep learning in healthcare. *CoRR* abs/1912.12115 (2019).
- [41] Xinchu Qiu, Ilias Leontiadis, Luca Melis, Alex Sablayrolles, and Pierre Stock. 2023. EXACT: Extensive Attack for Split Learning. *CoRR* abs/2305.12997 (2023).
- [42] Reza Shokri, Marco Stronati, Congzheng Song, and Vitaly Shmatikov. 2017. Membership inference attacks against machine learning models. In *S&P*. 3–18.
- [43] Abhishek Singh, Praneeth Vepakomma, Otkrist Gupta, and Ramesh Raskar. 2019. Detailed comparison of communication efficiency of split learning and federated learning. *CoRR* abs/1909.09145 (2019).
- [44] Nitish Srivastava, Geoffrey Hinton, Alex Krizhevsky, Ilya Sutskever, and Ruslan Salakhutdinov. 2014. Dropout: a simple way to prevent neural networks from overfitting. *JMLR* 15, 1 (2014), 1929–1958.
- [45] Gábor J Székely, Maria L Rizzo, and Nail K Bakirov. 2007. Measuring and testing dependence by correlation of distances. *Ann. Stat.* 35, 6 (2007), 2769.
- [46] Hassan Takabi, Ehsan Hesamifard, and Mehdi Ghasemi. 2016. Privacy preserving multi-party machine learning with homomorphic encryption. In *NeurIPS*.
- [47] Chandra Thapa, Mahawaga Arachchige Pathum Chamikara, and Seyit A Camtepe. 2021. Advancements of federated learning towards privacy preservation: from federated learning to split learning. *Federated Learning Systems: Towards Next-Generation AI* (2021), 79–109.
- [48] Praneeth Vepakomma, Otkrist Gupta, Tristan Swedish, and Ramesh Raskar. 2018. Split learning for health: Distributed deep learning without sharing raw patient data. *CoRR* abs/1812.00564 (2018).
- [49] Praneeth Vepakomma, Abhishek Singh, Otkrist Gupta, and Ramesh Raskar. 2020. NoPeek: Information leakage reduction to share activations in distributed deep learning. In *ICDM Workshops*. 933–942.
- [50] Praneeth Vepakomma, Abhishek Singh, Emily Zhang, Otkrist Gupta, and Ramesh Raskar. 2021. NoPeek-Infer: Preventing face reconstruction attacks in distributed inference after on-premise training. In *FG*. 1–8.

- [51] Zhou Wang, Alan C Bovik, Hamid R Sheikh, and Eero P Simoncelli. 2004. Image quality assessment: from error visibility to structural similarity. *IEEE Trans. Image. Process.* 13, 4 (2004), 600–612.
- [52] Alexander Wood, Kayvan Najarian, and Delaram Kahrobaei. 2020. Homomorphic encryption for machine learning in medicine and bioinformatics. *Comput. Surveys* 53, 4 (2020), 1–35.
- [53] Yuncheng Wu, Shaofeng Cai, Xiaokui Xiao, Gang Chen, and Beng Chin Ooi. 2020. Privacy preserving vertical federated learning for tree-based models. *PVLDB* 13, 12 (Jul 2020), 2090–2103.
- [54] Yuncheng Wu, Naili Xing, Gang Chen, Tien Tuan Anh Dinh, Zhaojing Luo, Beng Chin Ooi, Xiaokui Xiao, and Meihui Zhang. 2023. Falcon: A Privacy-Preserving and Interpretable Vertical Federated Learning System. *PVLDB* 16, 10 (2023), 2471–2484.
- [55] Han Xiao, Kashif Rasul, and Roland Vollgraf. 2017. Fashion-MNIST: a Novel Image Dataset for Benchmarking Machine Learning Algorithms. *CoRR abs/1708.07747* (2017).
- [56] Xiaokui Xiao, Guozhang Wang, and Johannes Gehrke. 2010. Differential privacy via wavelet transforms. *IEEE TKDE* 23, 8 (2010), 1200–1214.
- [57] Chengxu Yang, Qipeng Wang, Mengwei Xu, Zhenpeng Chen, Kaigui Bian, Yunxin Liu, and Xuanzhe Liu. 2021. Characterizing impacts of heterogeneity in federated learning upon large-scale smartphone data. In *WWW*. 935–946.
- [58] Andrew C. Yao. 1982. Protocols for secure computations. In *FOCS*. 160–164.
- [59] Xuefei Yin, Yanming Zhu, and Jiankun Hu. 2021. A comprehensive survey of privacy-preserving federated learning: A taxonomy, review, and future directions. *Comput. Surveys* 54, 6 (2021), 1–36.
- [60] Yupeng Yin, Xianglong Zhang, Huanle Zhang, Feng Li, Yue Yu, Xiuzhen Cheng, and Pengfei Hu. 2023. Ginver: Generative Model Inversion Attacks Against Collaborative Inference. In *WWW*. 2122–2131.
- [61] Jason Yosinski, Jeff Clune, Yoshua Bengio, and Hod Lipson. 2014. How transferable are features in deep neural networks?. In *NeurIPS*.
- [62] Xuejun Zhao, Wencan Zhang, Xiaokui Xiao, and Brian Lim. 2021. Exploiting explanations for model inversion attacks. In *ICCV*. 682–692.

A ADDITIONAL RELATED WORK

Split learning. Split learning (SL) [18, 40, 48] is a privacy preserving protocol for distributed training and inference of deep neural networks, and has gain increasing attention due to its simplicity, efficiency and scalability [24, 43, 47, 59]. Since its proposal, many works have extended SL to various configurations, including U-shaped SL that protects the client’s labels [18], SL with multiple clients with horizontal [48] or vertical [5] partition. We refer the audience to Sec. 2 and available surveys [24, 43, 47, 59] for more details on split learning.

Inference attacks against split learning. The security of SL has been a focus of the research community since the proposal of SL. Various privacy attacks have been proposed to infer clients’ labels or features under different threat models. Pasquini et al. [39] propose FSHA, an active feature inference attack where the server hijacks the gradients sent back to the client to control the updates of client’s private model. Erdoğan et al. [9] design passive feature and label inference attacks via alternating optimization of a surrogate model and inferred private inputs. Qiu et al. [41] also consider passive feature and label inference attacks, but with the extremely strong assumption that the server knows the model parameters of the victim clients, thus can utilize the excessive information on client’s model parameters and gradients. Concurrently with our work, Gao and Zhang [13] propose a passive feature and label inference attack against SL, namely PCAT, which adopts a similar framework as our naïve SDA discussed in the beginning of Sec. 4.1, with minor improvements such as label alignment and delayed training. On a separate line of research, several works [28, 30] focus solely on label inference attacks. This is not the focus of our work as we aim to develop effective attacks that can infer both the clients’ labels and features. At last, several attacks [22,

Algorithm 1 SDAR against vanilla split learning

Require: $\ell(\cdot, \cdot)$ is the loss function of the original SL task; s is the split level; η is the learning rate of the original SL task; $\eta_{\tilde{f}}, \eta_{\tilde{f}^{-1}}, \eta_{d_1}, \eta_{d_2}$ are learning rates for the server’s models $\tilde{f}, \tilde{f}^{-1}, d_1, d_2$ respectively.

```

1: procedure CLIENT:
2:   Initializes model  $f$  with parameters  $\theta_f$ 
3:   for  $i \in \{1, 2, \dots\}$  do
4:     Samples a batch of examples  $(X, Y) \in D$ 
5:      $Z_s \leftarrow f(X)$ 
6:     Sends  $(Z_s, Y)$  to the server ▷ Timestamp  $t_{i1}$ 
7:     Receives  $\nabla\theta_{s+1}$  from the server ▷ Timestamp  $t_{i2}$ 
8:     Calculates  $\nabla\theta_f$  using  $\nabla\theta_{s+1}$ 
9:      $\theta_f \leftarrow \theta_f - \eta\nabla\theta_f$  ▷ Original SL task
10:
11: procedure SERVER:
12:   Initializes model  $g$  with parameters  $\theta_g$ 
13:   Initializes models  $\tilde{f}, \tilde{f}^{-1}, d_1, d_2$  with parameters  $\theta_{\tilde{f}}, \theta_{\tilde{f}^{-1}}, \theta_{d_1}, \theta_{d_2}$ 
14:   for  $i \in \{1, 2, \dots\}$  do
15:     Receives  $(Z_s, Y)$  from the client ▷ Timestamp  $t_{i1}$ 
16:      $\mathcal{L} = \ell(g(Z_s), Y)$ 
17:      $\nabla\theta_g \leftarrow \partial\mathcal{L}/\partial\theta_g$ 
18:     Sends  $\nabla\theta_{s+1}$  to the client ▷ Timestamp  $t_{i2}$ 
19:      $\theta_g \leftarrow \theta_g - \eta\nabla\theta_g$  ▷ Original SL task
20:
21:     Samples a batch of examples  $(X', Y') \in D'$ 
22:      $\mathcal{L}_{\tilde{f}} \leftarrow \ell(g(\tilde{f}(X')), Y') + \lambda_1 \cdot \ell_{\text{BCE}}(d_1(\tilde{f}(X'), Y'), 1)$ 
23:      $\mathcal{L}_{d_1} \leftarrow \ell_{\text{BCE}}(d_1(\tilde{f}(X'), Y'), 0) + \ell_{\text{BCE}}(d_1(Z_s, Y), 1)$ 
24:      $\mathcal{L}_{\tilde{f}^{-1}} \leftarrow \ell_{\text{MSE}}(X', \tilde{f}^{-1}(\tilde{f}(X'), Y'))$ 
25:        $+ \lambda_2 \cdot \ell_{\text{BCE}}(d_2(\tilde{f}^{-1}(Z_s, Y), Y), 1)$ 
26:      $\mathcal{L}_{d_2} \leftarrow \ell_{\text{BCE}}(d_2(\tilde{f}^{-1}(Z_s, Y), Y), 0) + \ell_{\text{BCE}}(d_2(X', Y'), 1)$ 
27:      $\nabla\theta_{\tilde{f}} \leftarrow \partial\mathcal{L}_{\tilde{f}}/\partial\theta_{\tilde{f}}; \theta_{\tilde{f}} \leftarrow \theta_{\tilde{f}} - \eta_{\tilde{f}}\nabla\theta_{\tilde{f}}$ 
28:      $\nabla\theta_{d_1} \leftarrow \partial\mathcal{L}_{d_1}/\partial\theta_{d_1}; \theta_{d_1} \leftarrow \theta_{d_1} - \eta_{d_1}\nabla\theta_{d_1}$ 
29:      $\nabla\theta_{\tilde{f}^{-1}} \leftarrow \partial\mathcal{L}_{\tilde{f}^{-1}}/\partial\theta_{\tilde{f}^{-1}}; \theta_{\tilde{f}^{-1}} \leftarrow \theta_{\tilde{f}^{-1}} - \eta_{\tilde{f}^{-1}}\nabla\theta_{\tilde{f}^{-1}}$ 
30:      $\nabla\theta_{d_2} \leftarrow \partial\mathcal{L}_{d_2}/\partial\theta_{d_2}; \theta_{d_2} \leftarrow \theta_{d_2} - \eta_{d_2}\nabla\theta_{d_2}$ 
31:
32:    $\hat{X} \leftarrow \tilde{f}^{-1}(X_s)$  ▷ Reconstructed private features

```

[60] have been proposed against split inference, often known as collaborative inference. However, split inference is more vulnerable as the intermediate representations are products of a fixed client’s model, while in training-time SL attacks, the server has to invert the output of a constantly updated client’s model. Therefore, attacks against split inference are not our focus in this work.

Privacy-preserving improvements of split learning. In response to the privacy vulnerabilities of SL, various privacy-preserving improvements have been proposed. U-shaped SL [18] enhances privacy by preventing label exposure to the server, although our work demonstrates that SDAR can still infer private labels with high accuracy. Targeting active hijacking attacks such as FSHA [39], Erdogan et al. [8], Fu et al. [12] detect and defend against the active manipulation of back-propagated gradients. Vepakomma et al. [49, 50] propose to improve the privacy of SL by minimizing the correlation between the private inputs and the shared representations via injecting a correlation regularization term to the loss function of the original SL task, which we investigate in Sec. 6.

Algorithm 2 Simulator decoding attack with adversarial regularization (SDAR) against U-shaped split learning

Require: $\ell(\cdot, \cdot)$ is the loss function of the original SL task; s, t are the split levels; η is the learning rate of the original SL task; $\eta_{\tilde{h}}, \eta_{\tilde{f}}, \eta_{\tilde{f}^{-1}}, \eta_{d_1}, \eta_{d_2}$ are learning rates for the server’s models $\tilde{h}, \tilde{f}, \tilde{f}^{-1}, d_1, d_2$ respectively. p is the label flipping probability. \mathcal{Y} is the set of all possible labels.

```

1: procedure CLIENT:
2:   Initialize models  $f, h$  with parameters  $\theta_f, \theta_h$ 
3:   for  $i \in \{1, 2, \dots\}$  do
4:     Samples a batch of examples  $(X, Y) \in D$ 
5:      $Z_s \leftarrow f(X)$ 
6:     Sends  $Z_s$  to the server                                ▶ Timestamp  $t_{i1}$ 
7:     Receives  $Z_t$  from the server                            ▶ Timestamp  $t_{i2}$ 
8:      $\mathcal{L} \leftarrow \ell(h(Z_t), Y)$ 
9:      $\nabla \theta_h \leftarrow \partial \mathcal{L} / \partial \theta_h; \theta_h \leftarrow \theta_h - \eta \nabla \theta_h$  ▶ Original SL task
10:    Sends  $\nabla \theta_{t+1}$  to the server                            ▶ Timestamp  $t_{i3}$ 
11:    Receives  $\nabla \theta_{s+1}$  from the server                        ▶ Timestamp  $t_{i4}$ 
12:    Calculates  $\nabla \theta_f$  using  $\nabla \theta_{s+1}$ 
13:     $\theta_f \leftarrow \theta_f - \eta \nabla \theta_f$                             ▶ Original SL task
14:
15: procedure SERVER:
16:   Initialize model  $g$  with parameters  $\theta_g$ 
17:   Initialize models  $\tilde{h}, \tilde{f}, \tilde{f}^{-1}, d_1, d_2$  w/ param.  $\theta_{\tilde{h}}, \theta_{\tilde{f}}, \theta_{\tilde{f}^{-1}}, \theta_{d_1}, \theta_{d_2}$ 
18:   for  $i \in \{1, 2, \dots\}$  do
19:     Receives  $(Z_s, Y)$  from the client                        ▶ Timestamp  $t_{i1}$ 
20:      $Z_t = g(Z_s)$ 
21:     Sends  $Z_t$  to the client                                ▶ Timestamp  $t_{i2}$ 
22:     Receives  $\nabla \theta_{t+1}$  from the client                    ▶ Timestamp  $t_{i3}$ 
23:     Calculates  $\nabla \theta_g$  using  $\nabla \theta_{t+1}$ 
24:      $\theta_g \leftarrow \theta_g - \eta \nabla \theta_g$                             ▶ Original SL task
25:     Sends  $\nabla \theta_{s+1}$  to the client                        ▶ Timestamp  $t_{i4}$ 
26:
27:   Samples a batch of examples  $(X', Y') \in D'$ 
28:    $\tilde{Y}'_i \leftarrow \begin{cases} Y'_i & \text{w.p. } 1 - p \\ \text{Uniform}(\mathcal{Y}) & \text{w.p. } p \end{cases}$  ▶ Label random flipping
29:    $\mathcal{L}_{\tilde{h}} \leftarrow \ell(\tilde{h}(g(\tilde{f}(X'))), \tilde{Y}')$ 
30:    $\mathcal{L}_{\tilde{f}} \leftarrow \ell(\tilde{h}(g(\tilde{f}(X'))), \tilde{Y}') + \lambda_1 \cdot \ell_{\text{BCE}}(d_1(\tilde{f}(X')), 1)$ 
31:    $\mathcal{L}_{d_1} \leftarrow \ell_{\text{BCE}}(d_1(\tilde{f}(X')), 0) + \ell_{\text{BCE}}(d_1(Z_s), 1)$ 
32:    $\mathcal{L}_{\tilde{f}^{-1}} \leftarrow \ell_{\text{MSE}}(X', \tilde{f}^{-1}(\tilde{f}(X'))) + \lambda_2 \cdot \ell_{\text{BCE}}(d_2(\tilde{f}^{-1}(Z_s)), 1)$ 
33:    $\mathcal{L}_{d_2} \leftarrow \ell_{\text{BCE}}(d_2(\tilde{f}^{-1}(Z_s)), 0) + \ell_{\text{BCE}}(d_2(X'), 1)$ 
34:
35:    $\nabla \theta_{\tilde{h}} \leftarrow \partial \mathcal{L}_{\tilde{h}} / \partial \theta_{\tilde{h}}; \theta_{\tilde{h}} \leftarrow \theta_{\tilde{h}} - \eta_{\tilde{h}} \nabla \theta_{\tilde{h}}$ 
36:    $\nabla \theta_{\tilde{f}} \leftarrow \partial \mathcal{L}_{\tilde{f}} / \partial \theta_{\tilde{f}}; \theta_{\tilde{f}} \leftarrow \theta_{\tilde{f}} - \eta_{\tilde{f}} \nabla \theta_{\tilde{f}}$ 
37:    $\nabla \theta_{d_1} \leftarrow \partial \mathcal{L}_{d_1} / \partial \theta_{d_1}; \theta_{d_1} \leftarrow \theta_{d_1} - \eta_{d_1} \nabla \theta_{d_1}$ 
38:    $\nabla \theta_{\tilde{f}^{-1}} \leftarrow \partial \mathcal{L}_{\tilde{f}^{-1}} / \partial \theta_{\tilde{f}^{-1}}; \theta_{\tilde{f}^{-1}} \leftarrow \theta_{\tilde{f}^{-1}} - \eta_{\tilde{f}^{-1}} \nabla \theta_{\tilde{f}^{-1}}$ 
39:    $\nabla \theta_{d_2} \leftarrow \partial \mathcal{L}_{d_2} / \partial \theta_{d_2}; \theta_{d_2} \leftarrow \theta_{d_2} - \eta_{d_2} \nabla \theta_{d_2}$ 
40:
41:    $\hat{X} \leftarrow \tilde{f}^{-1}(X_s)$  ▶ Reconstructed private features
42:    $\hat{Y} \leftarrow \tilde{h}(g(X_s))$  ▶ Inferred private labels

```

B PSEUDOCODE

We provide the pseudocode for SDAR in Alg. 1 for the vanilla SL setting and Alg. 2 for the U-shaped SL setting.

C ON COMPUTATIONAL COMPLEXITY

We assume that the total number of training iterations is N with a batch size of b . In each iteration, the server receives a batch of intermediate representations and updates its models accordingly. If

Table 8: Mean and standard deviation of reconstruction SSIM over 5 trials on CIFAR-10 at split levels 3–7 in vanilla SL.

lv.	3	4	5	6	7
SDAR	0.87 (0.02)	0.80 (0.03)	0.75 (0.02)	0.71 (0.03)	0.59 (0.02)
PCAT	0.72 (0.03)	0.63 (0.03)	0.52 (0.03)	0.40 (0.08)	0.22 (0.03)

Table 9: Effects of different sizes of the auxiliary data D' on SDAR performed on CIFAR-10 at split level 7 in vanilla SL.

$ D' / D $	1.0	0.5	0.2	0.1	0.05
Attack MSE	0.0216 (0.0014)	0.0224 (0.0017)	0.0237 (0.0017)	0.0235 (0.0015)	0.0274 (0.0016)

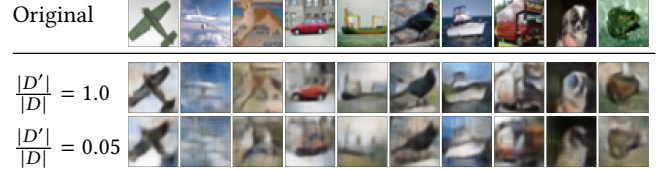


Figure 11: Examples of feature inference results of SDAR performed with auxiliary datasets of different sizes.

there’s no attack, the computation cost of the server only comes from the update of its own partial model, g , which is $2b \cdot |g|$ where $|g|$ denotes the number of parameters of the model g (coefficient 2 comes from the forward pass and backpropagation over g). If the server is to reconstruct the target training images via naïve SDAR, i.e., with an additional simulator \tilde{f} and a decoder \tilde{f}^{-1} , the additional computation cost will be $2b|\tilde{f}| + b|g| + 2b|\tilde{f}^{-1}|$, due to the forward pass on $\tilde{f}, g, \tilde{f}^{-1}$ and the updates to \tilde{f} and \tilde{f}^{-1} . Furthermore, if the server adopts full SDAR and introduces discriminators d_1, d_2 , additional cost of $2b|d_1| + 2b|d_2|$ will be introduced. Here, no extra cost is accounted towards the backpropagation of \tilde{f} and \tilde{f}^{-1} caused by adversarial regularization because these two models are only updated once, and the regularization terms are captured within their loss functions. Therefore, the total cost of SDAR over N iterations will be $bN(3|g| + 2|\tilde{f}| + 2|\tilde{f}^{-1}| + 2|d_1| + 2|d_2|)$, with an $O(1)$ cost per iteration if the batch size and model sizes are considered constants. Hence, SDAR is computationally efficient compared to UnSplit [9] by avoiding the inner loops for iterative optimization to attack in every single iteration and is asymptotically as efficient as PCAT [13], which adopts a similar attack framework as naïve SDAR.

D ADDITIONAL DISCUSSIONS**D.1 Evaluation on other metrics**

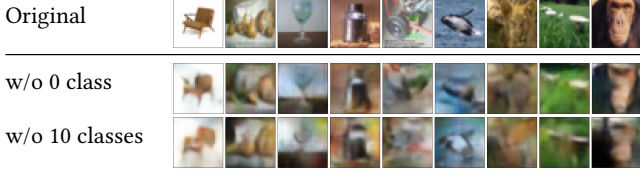
Following [12, 13], we evaluate SDAR and PCAT via Structural Similarity (SSIM) Index [51] in Table 8. We observe the same trends that SDAR reconstructs images of better quality than PCAT.

D.2 Effects of auxiliary data

Naturally, one is curious to ask if the proposed attacks are still effective when the server cannot curate a large auxiliary dataset that shares the same distribution as the client’s dataset. We hereby discuss the effects of the size and distribution of D' on SDAR.

Table 10: Effects of the removal of classes from D' on SDAR performed on CIFAR-100 at split level 7 in vanilla SL.

#classes removed	0	1	5	10
Attack MSE	0.0217 (0.0011)	0.0213 (0.0007)	0.0256 (0.0029)	0.0348 (0.0021)

**Figure 12: Examples of feature inference results of SDAR performed with auxiliary datasets with classes removed.**

We report the attack performance of SDAR with different sizes of auxiliary dataset D' in Table 9. We only observe a limited effect of the shrinkage of the auxiliary dataset on the performance of SDAR, as the attack MSE only slightly increases when D' shrinks. Fig. 11 also demonstrates precise reconstructions even with auxiliary data of size 5% of the client’s dataset. As for the effects of distributional discrepancies between D' and D , we experiment with SDAR on CIFAR-100 while removing examples of up to ten classes from the auxiliary dataset in Table 10. With the removal of more classes in D' , the attack performance degrades, but to a limited extent. Fig. 12 demonstrates that SDAR can still reconstruct images of good quality even when 10 classes are missing in the auxiliary dataset.

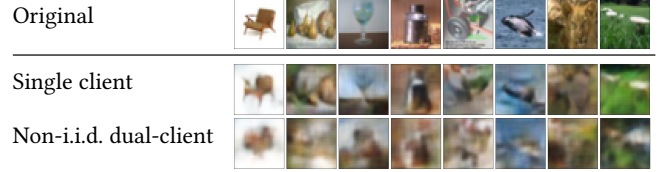
Intuitively, with D' of smaller size or with missing classes, one would expect the simulator/decoder trained on D' to be more prone to overfitting and thus learn less useful information about client’s private data. However, the core idea of SDAR is to reduce such overfitting by adversarial regularization. The positive results presented in this section demonstrate the effectiveness of adversarial regularization and show that SDAR can still work effectively even with a limited size of additional data, or with a substantial distributional discrepancy between D' and D .

D.3 Effects of simulator architecture

We have assumed that the server knows the architecture of the client’s partial model f and can initialize a simulator with identical architecture. Although this is a realistic assumption in practice, it is interesting to investigate whether SDAR still has superior attack performance when the server does not know the architecture of f . To this end, we conduct additional experiments on CIFAR-10 with SDAR and PCAT [13] in vanilla SL, where the server only knows the input and output dimensions of f . In particular, we continue to use the standard ResNet-20 model for f and g , but we use plain convolutional layers for the server’s simulator \tilde{f} . We report the attack performance of SDAR and PCAT in Table 11. We observe that the attack performance is sometimes slightly worse than the scenario where the server’s simulator shares an identical architecture as the client’s model, but SDAR is still effective in reconstructing high-quality training examples and outperforms PCAT by a large margin. This demonstrates that our proposed method is still effective even when the server does not know the architecture of f .

Table 11: Mean values with standard deviations of the reconstruction MSE over 5 trials on CIFAR-10 in the vanilla SL with or without access to the architecture of f .

lv.	Same architecture		Different architecture	
	SDAR	PCAT [13]	SDAR	PCAT [13]
3	0.0059 (0.0005)	0.0202 (0.0026)	0.0077 (0.0014)	0.0231 (0.0054)
4	0.0104 (0.0009)	0.0237 (0.0021)	0.0101 (0.0007)	0.0257 (0.0034)
5	0.0120 (0.0003)	0.0337 (0.0048)	0.0145 (0.0012)	0.0289 (0.0038)
6	0.0134 (0.0007)	0.0382 (0.0062)	0.0186 (0.0022)	0.0433 (0.0114)
7	0.0216 (0.0014)	0.0568 (0.0062)	0.0260 (0.0010)	0.0545 (0.0039)

**Figure 13: Examples of feature inference results of SDAR performed in single client vs heterogeneous dual-client settings on CIFAR-100 at split level 7 in the vanilla SL setting.**

D.4 Multi-client scenarios

We have discussed inference attacks on SL in the context of a single-client setting. However, in practice, the server often serves multiple clients, each with their own private data. Our methods, SDAR, can be directly applied to multi-client scenarios because in multi-client SL, each client sends its own batch of intermediate representations to the server in return for gradients to be sent back. From the server’s perspective, it sees sequentially incoming batches of intermediate representations, which is the same regardless whether the batches are coming from distinct clients or a single one, and can attack the received batch of data using our proposed method, SDAR. If all clients hold i.i.d. data, each client sampling a batch of its own data is equivalent to a single “virtual client” sampling a batch of data from the combined data pool, and our attacks are readily applicable to this scenario and no performance loss is expected.

In the multi-client scenario where different clients possess heterogeneous data distributions, we conduct additional evaluations of SDAR under a two-client setting to provide some insights. In this setting, one client holds 50 classes of CIFAR-100, while the other holds the other 50 classes. And they alternately interact with the server. We run SDAR under this two-client setting at a split level of 7 for five trials, resulting in an average attack MSE of 0.0415, with a standard deviation of 0.0093. This is relatively worse than the attack performance under the i.i.d. setting, but as shown in Fig. 13, SDAR can still reconstruct some visual features of the private data.

The performance degradation could be attributed to the fact that in the non-i.i.d. setting, the updates from different clients are not homogeneous, which may result in issues with the convergence of partial models, thus a worse simulator on the server side. We argue that to better solve this issue, new attack techniques should be explored, and we leave the thorough investigation of the heterogeneous multi-client setting to future work.

E ADDITIONAL POTENTIAL DEFENSES

Homomorphic encryption. One of the most straightforward ideas to mitigate privacy issues in SL is to encrypt the intermediate representations Z_s and send only the ciphertext to the server such that the server cannot use it to infer private features. This usually requires homomorphic encryption (HE) [46, 52] where the server can only perform computation on the ciphertext without decrypting it and return the ciphertext of the result to the client. In the context of SL, this means that the server must execute forward pass, loss evaluation, and backward propagation all in ciphertext, and at last sends the gradients $\nabla\theta_{s+1}$ in ciphertext back to the client. However, current HE schemes usually only support homomorphic arithmetic operations such as addition and multiplication, and it is computationally prohibitive to execute the forward pass and backward propagation in ciphertext, which typically involves non-linear operations and necessitates the use of approximation techniques [46]. Therefore, homomorphic encryption can hardly be applicable to SL, especially for deep neural network models.

Secure multi-party computation. Another widely-used cryptographic technique to protect privacy is secure multi-party computation (MPC) [4, 25, 53, 58], where multiple parties jointly compute a function on their private inputs without revealing their inputs to each other. To the best of our knowledge, there has been no prior work improving the privacy of SL using MPC. Even if it is possible to apply MPC such that the client and the server can train their models without revealing private data of the client or model parameters of both parties, such protocol will introduce significant computational overhead and communication cost, completely defeating the purpose and promises of split learning.

Differential privacy. Currently, the state-of-the-art technique to quantify and reduce information disclosure about individuals is differential privacy (DP) [2, 7, 56], which mathematically bounds the influence of private data on the released information. In the context of SL, this would mean that the intermediate representations Z_s are differentially private with regard to the client’s private features X . If we are to achieve DP in split learning, random noise will be injected by the client, such that even if the client arbitrarily modifies the input data X , the intermediate representations Z_s will remain almost unchanged. That is, client’s model f will output similar representations for any input data, which practically renders the model trivial. Therefore, DP is not applicable to our problem.

F IMPLEMENTATION DETAILS

F.1 Experiment setup

The experiments are conducted on machines running Ubuntu 20.04 LTS, equipped with two Intel® Xeon® Gold 6326 CPUs, 256GB of RAM and an NVIDIA® A100 80GB GPU. We implement our attack and other baselines in Python and TensorFlow [6]. Our code base is available at https://anonymous.4open.science/r/SDAR_SplitNN/ for reproducibility.

F.2 Split learning setup

We target the same SL setup across all experiments, where the complete model H is ResNet-20 and we experiment with various split configurations of the model, as shown in Fig. 14. For all experiments, we use Adam optimizer [26] to optimize H (that is, $g \circ f$ in

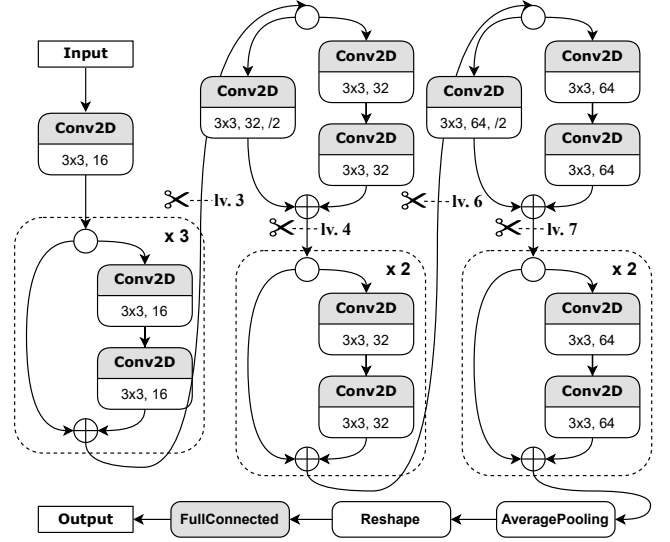


Figure 14: The ResNet-20 architecture and split configurations used in our experiments.

vanilla SL and $h \circ g \circ f$ in U-shaped SL) with default initial learning rate $\eta = 0.001$. We use 128 examples per batch as per the original ResNet paper suggests [21]. We train the model H with split learning protocol for 10000 iterations (i.e., batches) on Fashion-MNIST, and 20000 iterations on CIFAR-10, CIFAR-100, and Tiny ImageNet. For all attacks, on all datasets, at all considered split levels and under both vanilla and U-shaped settings, we run five trials for statistical significance.

F.3 Implementation details of SDAR

Models. Due to our threat model where the server knows the model architecture of $H = g \circ f$, the server uses the same model architecture for its simulator \tilde{f} as the client’s model f , but with random initialization. When experimenting with the relaxed assumption that the server does not know the architecture of the client model (e.g. in App. D.3), the server’s simulator is a plain residual network by removing the skip connections in the client’s residual network. Server’s decoder \tilde{f}^{-1} is a deep convolutional network, where each residual block of \tilde{f} corresponds to a deconvolution block (deconvolutional layer, followed by batch normalization and ReLU) in reverse order. Note that we replace deconvolutional layers with strides 2 with a combination of an upsampling layer and a convolutional layer, to reduce the checkerboard effects [36]. For MNIST dataset, we use a shallower network architecture, which skips the non-upsampling deconvolutional blocks. For the discriminator d_1 which distinguishes intermediate representations, we use a deep convolutional network with up to 256 filters, where each convolutional layer is followed by LeakyReLU and batch normalization except the last layer. The discriminator d_2 that distinguishes real and fake images follows a rather standard architecture, consists of convolutional layers, batch normalization and LeakyReLU. In the vanilla setting where labels are used as part of the input to the decoder and discriminators, we first transform the labels into embeddings of 50 units, and then further transform the embeddings by a learnable fully connected layer, before concatenating with

Table 12: Hyperparameters used in SDAR.

Setting	Dataset	λ_1	λ_2	η_h	p
Vanilla	All datasets	0.02	0.00002	NA	NA
U Shaped	Fashion-MNIST	0.04	0.0001	0.001	0.4
U Shaped	CIFAR-10	0.02	0.00001	0.001	0.2
U Shaped	CIFAR-100	0.04	0.00001	0.001	0.2
U Shaped	Tiny ImageNet	0.04	0.00001	0.001	0.2

the input to the decoder and discriminators. Details of the model architectures can be found in `src/models/attacker_models.py` of our code base.

Hyperparameters. All models are optimized with the Adam optimizer. As a simulator to f , we choose the learning rate of \tilde{f} the same as f , and we always keep the learning rate of the decoder half of that of the simulator, i.e., $2\eta_{\tilde{f}-1} = \eta_{\tilde{f}} = \eta$ for all cases. We choose smaller learning rates for the discriminators d_1, d_2 as this is the standard practice in GAN training. We choose the adversarial regularization factors λ_1, λ_2 such that $\lambda_1\eta_{\tilde{f}} = \eta_{d_1}$ and $\lambda_2\eta_{\tilde{f}} = \eta_{d_2}$, to ensure that the step size to minimize generator loss (as a regularization term) is on par with that of the discriminator loss. We use the same configuration for all experiments in vanilla SL across all datasets, while different configurations are chosen for different datasets in U-shaped SL. In particular, the hyperparameters used in the experiments are shown in Table 12.

F.3.1 Implementation details of baseline methods

PCAT. We implement PCAT [13] with the exact same model architectures for simulator and decoder as SDAR for a fair comparison. We also give the server in PCAT the same auxiliary dataset as SDAR. Compared to naïve SDA, PCAT uses two unique techniques to improve its performance. First, in vanilla SL where the server knows the labels of the private examples, PCAT aligns these labels by sampling auxiliary examples with the same labels as the received private examples. Second, in both vanilla and U-shaped SL, PCAT introduces a delay in attacking, where the server does not train its simulator and decoder until a certain number of iterations have been executed, to avoid the noisy early-stage training process disturbing the attacks. We implement both techniques, and choose a delay period of 100 iterations, as used in the original paper [13]. Note that by the time our research was conducted, the code of PCAT was not publicly available, so we implement PCAT from scratch based on the description in the original paper [13].

UnSplit. UnSplit [9] infers the private features X by minimizing $\ell_{\text{MSE}}(\tilde{f}(\hat{X}), Z_s)$ via alternating optimization of \tilde{f} and \hat{X} , where \tilde{f} is a surrogate model of the same architecture as f but randomly initialized, and \hat{X} is initialized as tensors filled with 0.5. We follow the implementation of the original paper [9] and use the same configuration for the alternating optimization algorithm. We use Adam optimizer with learning rate of 0.001 for both \tilde{f} and \hat{X} . The alternating optimization process consists of 1000 rounds, each having 100 \tilde{f} optimization steps and 100 \hat{X} optimization steps. Following [9], total variation is used to regularize the optimization of \hat{X} . In each training iteration of SL, UnSplit is able to infer the private training examples X by running the iterative alternating optimization procedure. However, due to the extremely high computational

Table 13: Extended tables and figures and their corresponding versions in the main text.

Figure/table in main text	Extended figure/table
Table 2	Table 14
Fig. 4a	Fig. 16
Fig. 5	Fig. 17
Fig. 6	Fig. 18
Table 4	Table 15 and 16
Fig. 7a	Table 20

cost of the iterative optimization process, we are unable to run the optimization algorithm for every training iteration, but only attack the last batch of training examples.

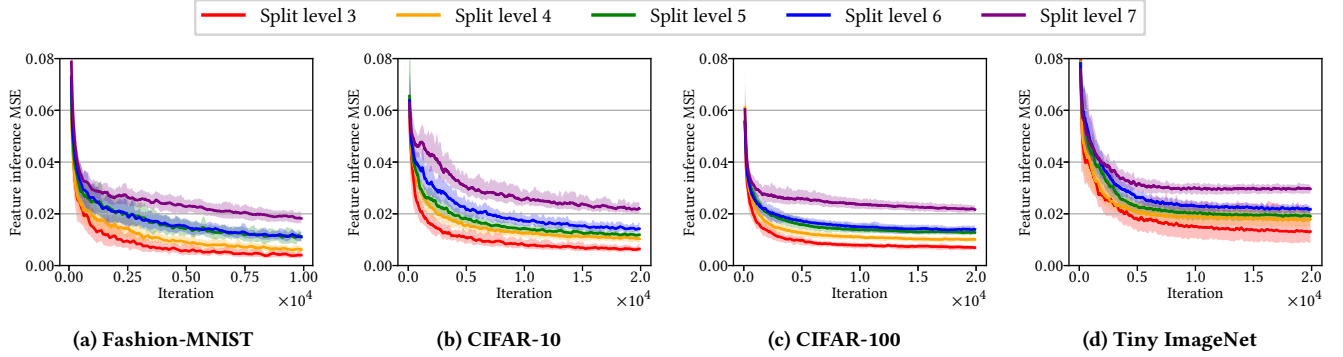
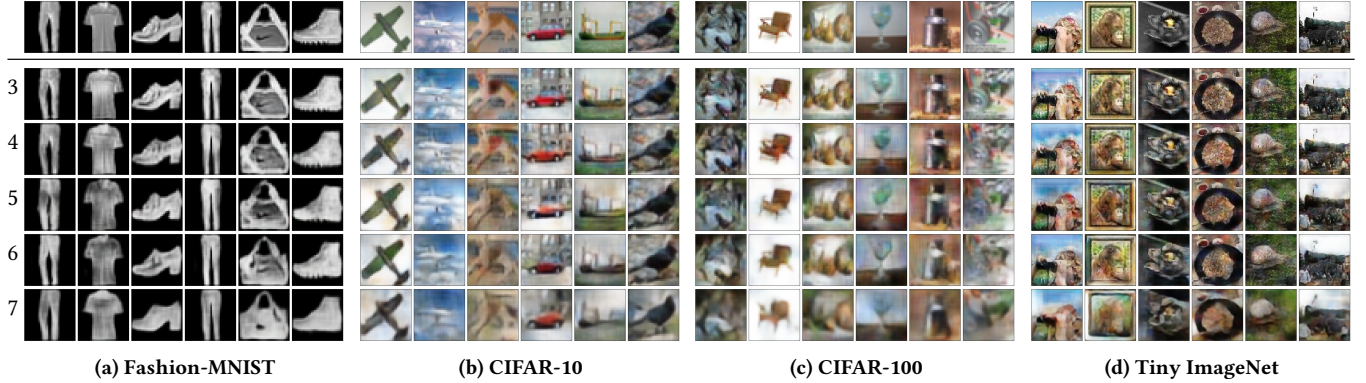
FSHA. We implement FSHA [39] with the same model architectures for the encoder, decoder and simulator discriminator as SDAR for a fair comparison, with the exception that we remove batch normalization layers in the simulator discriminator model as FSHA utilizes Wasserstein GAN loss with gradient penalty (WGAN-GP) [17]. In FSHA, the client’s model f is hijacked by the server to be updated to simulate the behaviors of the server’s own encoder \tilde{f} . Following the original paper, we use learning rate 0.00001 for the training of f as a generator and use learning rate 0.0001 for the discriminators with gradient penalty coefficient of 500 [17]. The encoder and decoder are trained in an autoencoder fashion [23] with learning rate 0.00001.

G FULL EXPERIMENTAL RESULTS

In Sec. 5, we only present experimental results on a single dataset due to limited space. We hereby provide the full results of our experiments on all four datasets as well as some additional experiments and discussions. We list all extended tables and figures and their corresponding versions in the main text in Table 13. In addition, we also report the attack MSE (and label inference accuracy for U-shaped SL) of SDAR over training iterations across all split configurations on all datasets in Fig. 15 and 19 for vanilla and U-shaped SL respectively.

Table 14: Mean and standard deviation of feature inference attack MSE on all datasets at split levels 3–7 in vanilla SL.

Dataset	Method	Split Level				
		3	4	5	6	7
Fashion-MNIST	SDAR	0.0039 (0.0007)	0.0062 (0.0008)	0.0102 (0.0011)	0.0113 (0.0016)	0.0178 (0.0012)
	PCAT	0.0248 (0.0129)	0.0245 (0.0028)	0.0308 (0.0045)	0.0524 (0.0059)	0.0756 (0.0046)
	UnSplit	0.1302 (0.0092)	0.1394 (0.0080)	0.1496 (0.0024)	0.1514 (0.0010)	0.1502 (0.0007)
CIFAR-10	SDAR	0.0059 (0.0005)	0.0104 (0.0009)	0.0120 (0.0003)	0.0134 (0.0007)	0.0216 (0.0014)
	PCAT	0.0202 (0.0026)	0.0237 (0.0021)	0.0337 (0.0048)	0.0382 (0.0062)	0.0568 (0.0062)
	UnSplit	0.0688 (0.0027)	0.0662 (0.0004)	0.0670 (0.0000)	0.0674 (0.0005)	0.0660 (0.0000)
CIFAR-100	SDAR	0.0067 (0.0005)	0.0101 (0.0007)	0.0128 (0.0012)	0.0136 (0.0011)	0.0217 (0.0011)
	PCAT	0.0151 (0.0021)	0.0185 (0.0032)	0.0244 (0.0028)	0.0300 (0.0014)	0.0430 (0.0014)
	UnSplit	0.0846 (0.0070)	0.0726 (0.0008)	0.0728 (0.0004)	0.0730 (0.0000)	0.0718 (0.0004)
Tiny ImageNet	SDAR	0.0130 (0.0052)	0.0180 (0.0023)	0.0189 (0.0017)	0.0221 (0.0004)	0.0295 (0.0011)
	PCAT	0.0384 (0.0058)	0.0390 (0.0083)	0.0400 (0.0024)	0.0439 (0.0038)	0.0484 (0.0026)
	UnSplit	0.0758 (0.0004)	0.0778 (0.0004)	0.0790 (0.0000)	0.0796 (0.0005)	0.0780 (0.0000)

**Figure 15: Feature inference attack MSE of SDAR over training iterations at split levels 3–7 on vanilla SL****Figure 16: Examples of feature inference attack results of SDAR all datasets at split levels 3–7 in vanilla SL.**

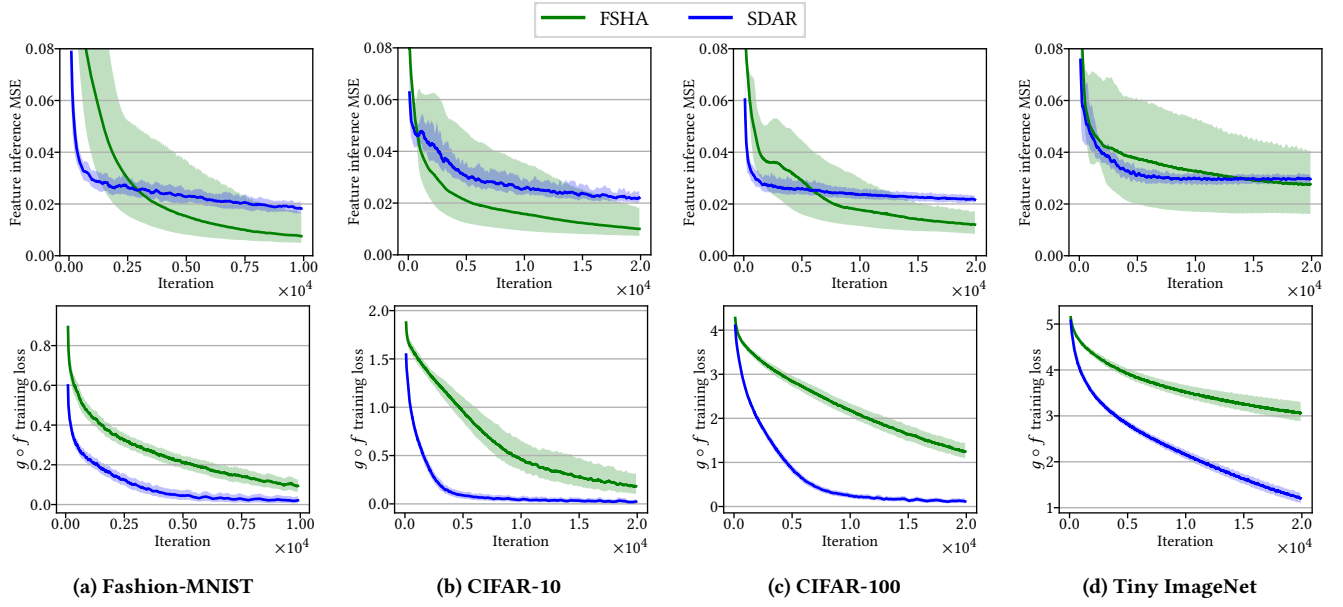


Figure 17: Attack MSE (upper) and original task training loss (lower) of SDAR vs FSHA on all datasets at level 7 in vanilla SL.

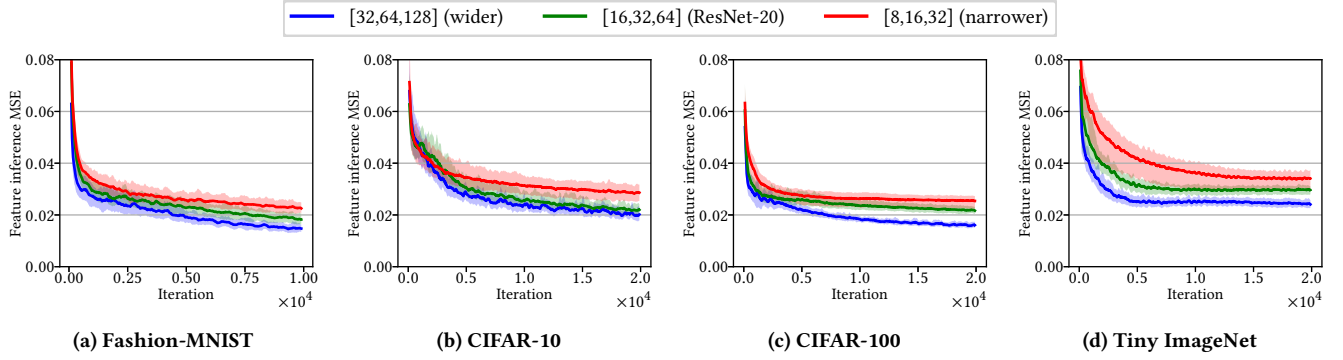


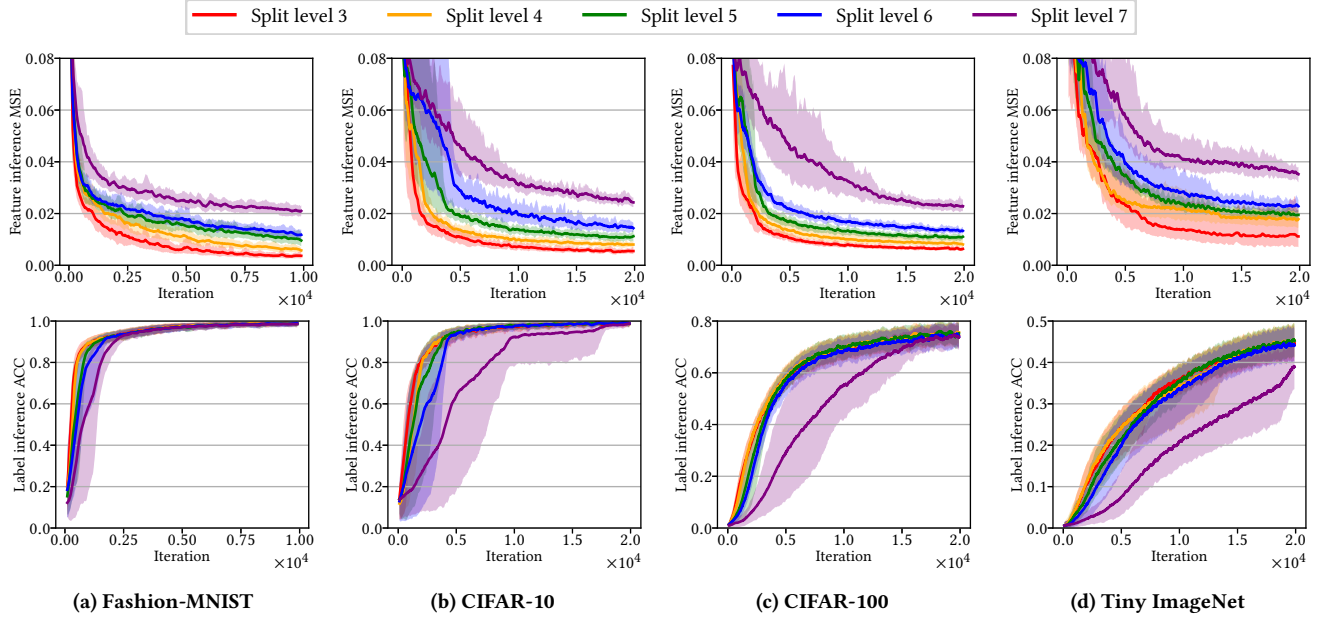
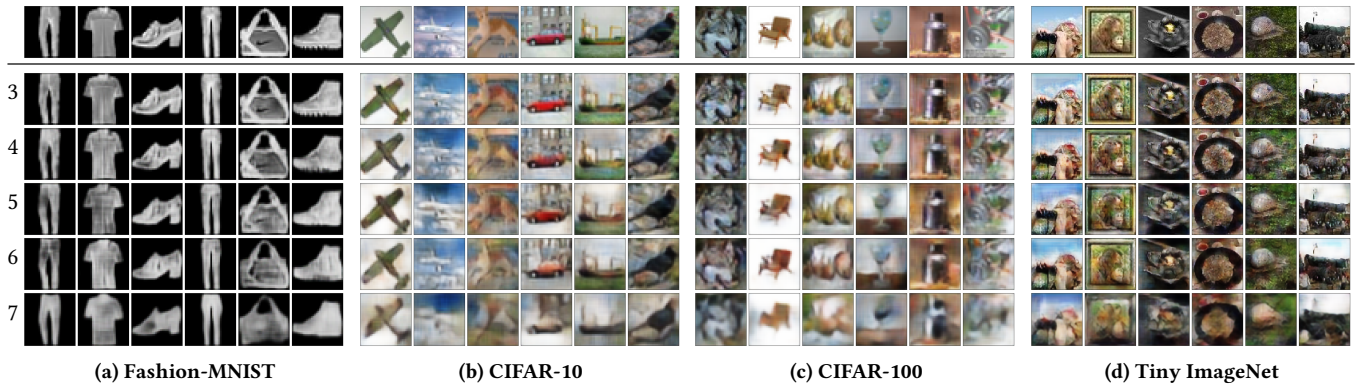
Figure 18: Attack MSE of SDAR on all datasets at split level 7 in vanilla SL with different model widths

Table 15: Mean and standard deviation of feature inference attack MSE on all datasets at split levels 3–7 in U-shaped SL.

Dataset	Method	Split Level				
		3	4	5	6	7
Fashion-MNIST	SDAR	0.0030 (0.0005)	0.0059 (0.0012)	0.0093 (0.0016)	0.0115 (0.0014)	0.0211 (0.0011)
	PCAT	0.0500 (0.0408)	0.0946 (0.0175)	0.1290 (0.0094)	0.1036 (0.0159)	0.1308 (0.0102)
CIFAR-10	SDAR	0.0051 (0.0007)	0.0085 (0.0013)	0.0120 (0.0017)	0.0138 (0.0013)	0.0247 (0.0009)
	PCAT	0.0223 (0.0040)	0.0387 (0.0262)	0.0665 (0.0262)	0.0791 (0.0122)	0.0947 (0.0184)
CIFAR-100	SDAR	0.0067 (0.0012)	0.0084 (0.0015)	0.0115 (0.0010)	0.0132 (0.0006)	0.0227 (0.0007)
	PCAT	0.0453 (0.0492)	0.0547 (0.0418)	0.0708 (0.0200)	0.0998 (0.0091)	0.0938 (0.0062)
Tiny ImageNet	SDAR	0.0111 (0.0059)	0.0184 (0.0031)	0.0192 (0.0015)	0.0223 (0.0025)	0.0348 (0.0020)
	PCAT	0.0456 (0.0196)	0.0551 (0.0386)	0.0764 (0.0259)	0.0913 (0.0270)	0.1085 (0.0102)

Table 16: Mean and standard deviation of label inference accuracy on all datasets at split levels 3–7 in U-shaped SL.

Dataset	Method	Split Level				
		3	4	5	6	7
Fashion-MNIST	SDAR	98.33 (0.19)	98.66 (0.15)	98.17 (0.49)	98.91 (0.40)	98.49 (0.37)
	PCAT	76.40 (34.46)	22.48 (26.25)	13.88 (3.88)	19.91 (14.88)	10.40 (7.33)
CIFAR-10	SDAR	98.15 (1.18)	98.61 (0.26)	98.49 (0.25)	98.15 (0.51)	98.71 (0.77)
	PCAT	98.13 (1.16)	88.66 (18.88)	58.11 (34.33)	21.34 (25.29)	15.45 (9.99)
CIFAR-100	SDAR	73.48 (1.70)	75.16 (1.46)	74.84 (1.63)	73.72 (2.36)	73.83 (1.20)
	PCAT	61.98 (27.02)	45.33 (33.78)	16.91 (18.71)	3.44 (2.51)	2.32 (1.75)
Tiny ImageNet	SDAR	41.93 (0.65)	41.22 (1.16)	42.27 (0.58)	41.50 (0.44)	37.19 (2.36)
	PCAT	37.12 (7.55)	33.32 (15.90)	15.89 (8.53)	13.83 (14.63)	0.98 (0.36)

**Figure 19: Feature inference attack MSE (upper) and label inference accuracy (lower) of SDAR over training iterations at split levels 3–7 on U-shaped SL****Figure 20: Examples of feature inference attack results of SDAR all datasets at split levels 3–7 in U-shaped SL.**